University of Oxford

M.Sc. Mathematical Modelling and
Scientific Computing

Nonlinear Waves in Granular Lattices

Author:
Michael P. Byrne

Supervisor:
Dr Mason A. Porter

2009

Acknowledgements

I would like to thank my dissertation supervisor, Dr Mason Porter, for his direction, suggestions and generous support throughout.

I would also like to acknowledge Dr Georgios Theocharis for his helpful suggestions and for permission to use his code for the simulations with discrete breathers.

This publication was based on work supported in part by Award No KUK-C1-013-04 , made by King Abdullah University of Science and Technology (KAUST).

Abstract

We present a numerical study of solitary waves in one dimensional (1D) granular lattices. Our system consists of an array of deformable spheres which we model using Hertzian interactions between neighbouring bodies. A general discussion of the origin of solitary waves is presented. We then provide an analysis of the Hertz force. For the case of a uniform chain of spheres, we derive an approximate solution in the asymptotic limit to the system equations. The solution is a solitary wave and numerical simulations verify this result. A scaling analysis is used to determine a relation between wave speed and amplitude. We find $v_s \propto F_{\mathrm{peak}}^{1/6}$, where v_s is the wave speed and F_{peak} the amplitude and this is corroborated using simulations. We then proceed from uniform chains to those containing a defect. A study of the effect of defect size and material properties (*i.e.* Young's modulus E and Poisson ratio ν) on a propagating solitary wave is performed. Finally, we outline the origin of intrinsic localised modes in granular lattices. These objects cause the scattering of incoming waves which can lead to interesting resonance phenomena. We probe the interaction of both solitary and plane waves with these modes. The transmission coefficient for plane waves is measured as a function of wavenumber q in order to observe whether the system permits behaviour analogous to Fano resonance. The results obtained do not clearly correspond to the Fano resonances observed in other systems. Thus, further studies are required to explain the mechanism of a plane wave's interaction with a localised mode.

Contents

1 Introduction

This dissertation investigates the dynamics of a one dimensional chain of spherical balls. The system can be modelled as a series of coupled nonlinear oscillators, and as such exhibits many fascinating phenomena such as solitary waves [22] and intrinsic localized modes [8]. Studies of nonlinear oscillator chains began over fifty years ago with the Fermi-Pasta-Ulam (FPU) problem and today it is still an active area of research [27].

One of the most interesting properties of these chains of nonlinear oscillators is that they support the propagation of solitary waves. Waves of this type are examples of nonlinear waves. Nonlinear waves have been studied since the nineteenth century, for example by Stokes, Korteweg and deVries, Boussinesq, and others [30]. Specifically, the solitary wave discovered experimentally by John Scott Russell on a Scottish canal in the 1830s was shown to be a solution to the following equation

$$\psi_t + (c_0 + c_1\psi)\psi_x + \nu\psi_{xxx} = 0. \tag{1.1}$$

In this equation, ψ denotes the displacement, the subscripts x and t indicate partial derivatives with respect to those quantities, and c_0, c_1 and ν are constants. This equation was initially introduced by Korteweg and deVries to describe long waves in water of relatively shallow depth. However, Equation (1.1), known as the *KdV equation*, has since been applied to other systems due to it being one of the simplest equations to combine nonlinearity and dispersion. The effect of these phenomena is discussed in detail in Chapter 2. However, the KdV equation is not alone in having solitary wave solutions - the *sine-Gordon* and *nonlinear Schrödinger* equations have also been found to yield such waves.

Solitary waves have been discovered in a variety of physical contexts, from optics to waterways and many others. A recently observed occurrence is in a system of discrete, barely touching spheres which interact via the nonlinear Hertz force (see Section 2.4.1). Solitary waves in these Hertzian lattices were first investigated by Nesterenko [23] and have since been probed by experiments [3], numerical simulations [12], and by analytical calculations [2]. Such a system is of interest for a variety of reasons: from understanding

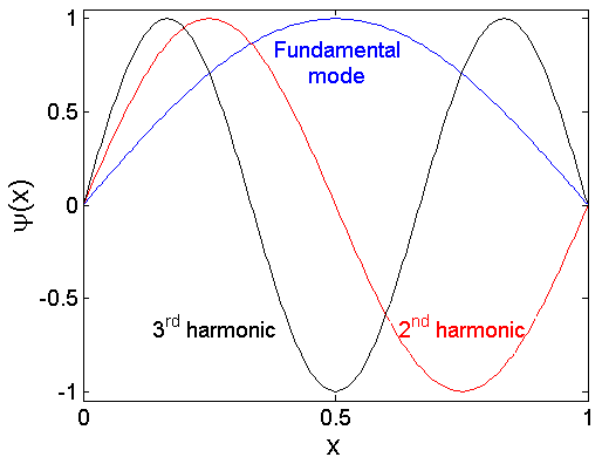

Figure 1.1: The displacement $\psi(x)$ for a string fixed at both ends (*i.e.* at $x = 0$ and $x = 1$) is given by $\psi(x) = A\sin(n\pi x)$, where the amplitude A is set to one and n is an integer. The first three modes of vibration, corresponding to $n = 1$, 2, 3, are shown in this diagram.

the basic physics of the wave propagation, to investigating the role of defects, and also potential industrial applications. As mentioned above, the study of nonlinear granular lattices was inspired by the FPU problem and we now describe this groundbreaking research.

At the Los Alamos Scientific Laboratory in 1955, Enrico Fermi, John Pasta and Stanislaw Ulam introduced a model consisting of a chain of nonlinear oscillators [7]. They were interested in studying the equilibration of energy among the different modes in the system. We can explain the concept of modes by considering a string fixed at both ends. When the string is plucked it will vibrate. There are an infinite number of vibration modes at which the string may oscillate (see Figure 1.1). The first mode is the fundamental mode, followed by the second harmonic, third harmonic and so on. A string is a linear system and so if a vibration is set up at, say, the fundamental frequency then this mode will continue to oscillate for all time (neglecting dispersion and assuming the vibration is undamped). The reason for this is that the individual modes cannot interact with each other. In a nonlinear system however, mode-mode interactions are possible. This allows energy to be transferred between modes. FPU assumed that their system, after a certain period of time, would thermalise *i.e* the energy of the sys-

tem would eventually be equipartioned between all the modes in the system. However, after running simulations on their system they did not observe equipartioning. To the astonishment of the researchers, the results showed that although energy was initially shared between a number of modes, after a period of time the system returned to a state that was close to the initial state. In the 1960s the connection between the FPU problem and the work performed on nonlinear waves by Korteweg-de Vries and others, was made by Norman Zabusky and Martin Kruskal. Introducing a continuum model of the FPU system, they realised that the partial differential equation describing the motion of the system was, in fact, the KdV equation which had originally been derived more than sixty years previously. The solutions they found were a particular type of solitary wave which they called a *soliton*[1]. Although the motion of solitons in an FPU chain can be quite regular, the system can also show chaotic behaviour depending on the initial conditions. If the energy provided to the system is sufficiently high then chaos can allow energy to be transferred between modes leading to equipartition. The complex behaviour and striking nonlinear effects observable in this seemingly simple system have inspired extensive research and this problem is still being investigated today [26].

Our investigations will begin with a system that is very similar to the original FPU setup. We will examine the properties of a uniform chain of spheres. The Hertz force will be introduced and an approximate solution to the equations of motion of the system will be derived. We will also solve the system numerically.

In Chapter 3, we introduce a defect to our lattice. Such impurities can dramatically alter the behaviour of the granular chain. Using numerical simulations, we vary the properties of this defect and investigate the effects on the propagation of the solitary wave.

In addition to solitary waves, Hertzian systems have also been shown to support intrinsic localised modes (ILMs), which are also known as discrete breathers (DBs) [28]. These are spatially localised solutions to the equations of motion which arise due to the combination of nonlinearity and discreteness

[1]The commonly used term *soliton* is a special case of a solitary wave. Solitons have an additional amazing property which is that if two solitons collide they retain their properties and emerge intact [19].

in the system (see Section 4.3). Chapter 4 focuses on the interaction of solitary and plane waves with a DB. Motivated by the observation of Fano resonances in waveguide arrays [21], we numerically investigate the possibility of a nonlinear "Fano-like" resonance due to the interaction of plane waves with the DB. We term such a resonance as Fano-like because Fano resonance itself is a linear phenomenon, this will be explored further in Chapter 4.

We end with our conclusions followed by the Appendices which contain the MATLAB codes used to perform the simulations for Chapters 2 and 3.

2 Solitary Waves in Hertzian Chains

2.1 What is a Solitary Wave?

In this chapter, we will begin by introducing the concept of nonlinear waves and explaining how they arise. Following that, a description of the granular lattice system that is the focus of this dissertation will be given. We will then derive an approximate solution to the system's equations of motion before presenting the results of numerical simulations. In addition, we include a brief discussion of the techniques used to investigate these systems experimentally.

As mentioned in Chapter 1, a 1D chain of spherical balls may support the propagation of a solitary wave. Solitary waves are fundamentally different to most of the waves we encounter in everyday life. Most waves, such as sound waves and electromagnetic waves, are linear waves. Linear waves are characterised by having a return force which is linearly dependent on the displacement. Solitary waves, however, are nonlinear waves - the return force is not directly proportional to the displacement from equilibrium [19]. This can be illustrated more clearly by considering the equation for a sinusoidal travelling wave, which we write as

$$u(x,t) = A\sin(qx - \omega t + \phi) \tag{2.1}$$

where u is the displacement from equilibrium, A is the wave amplitude, q the wave number, ω the angular frequency and ϕ an initial phase shift. We know that $\omega = vq$ where v is the wave speed. An important point to note is that Equation (2.1) is a solution to the equation for a harmonic oscillator, *i.e.*

$$\ddot{u}(x,t) \equiv \frac{\mathrm{d}^2 u}{\mathrm{d}t^2} = -\omega^2 u(x,t) \tag{2.2}$$

where the dot represents the derivative with respect to time. This equation shows that the restoring force is linearly dependent on the displacement. Another important property of linear waves is that the wave speed is independent of the wave amplitude, it depends only on the properties of the material through which it passes [27].

However, not all return forces are linear. We will consider nonlinear forces of the form

$$\ddot{u} = k(u^{\alpha}), \qquad \alpha > 1 \tag{2.3}$$

where k is a constant. Such nonlinear forces, combined with a phenomenon known as *dispersion* (we will give a detailed discussion of dispersion in Section 2.2) can allow solitary waves to propagate in a given medium and this will be illustrated in Section 2.3.

2.2 Wave Dispersion

In order to understand the origin of solitary waves, we must explain the phenomenon of dispersion. A dispersive system is one in which the velocity of a wave depends on its frequency. This dependence is expressed by a *dispersion relation* that relates ω to q for a particular system.

2.2.1 Non-Dispersive Waves

First, we will consider non-dispersive waves. The non-dispersive wave equation is written as

$$\frac{\partial^2 u}{\partial t^2} = v^2 \frac{\partial^2 u}{\partial x^2}. \tag{2.4}$$

This equation admits travelling wave solutions. A particular class of these solutions are sinusoidal travelling waves, an example of which is given by Equation (2.1). Sinusoidal travelling waves are just a subset of the *d'Alembert solutions* to Equation (2.4). D'Alembert's general solution to Equation (2.4) is written as

$$u(x,t) = F(x+vt) + G(x-vt) \tag{2.5}$$

where F and G are functions. This solution is interpreted as two waves with speed v moving in opposite directions along the x-axis.

We use sinusoidal waves as an example to highlight the properties of non-dispersive systems. These solutions can also be expressed as

$$u(x,t) = C\exp[\mathrm{i}(\omega t - qx)] + C^*\exp[-\mathrm{i}(\omega t - qx)] \tag{2.6}$$

where C is a constant (with complex conjugate C^*). Inserting this expression into Equation (2.4) we see that in order for the solution to be valid, ω and

q must satisfy $\omega = \pm vq$. If we consider waves described by Equation (2.6) to be travelling along a piece of string, for instance, then it is obvious that each point on the string vibrates at the same angular frequency ω. Another important property of these waves is the *phase velocity* v_ϕ. For sinusoidal travelling waves, v_ϕ is given by [19]

$$\frac{\mathrm{d}x}{\mathrm{d}t} = \frac{\omega}{q} \equiv v_\phi. \tag{2.7}$$

This quantity describes the velocity at which the entire wave profile moves. For the waves we are currently discussing, v_ϕ depends only on the properties of the medium and not on the properties of the wave itself, such as its frequency. For a sinusoidal travelling wave, constant values of the phase angle move either to the left or to the right (if we consider a string, for example) with a velocity v. As d'Alemberts solution (2.5) shows, this behaviour can be generalized to non-sinusoidal waves which do not undergo harmonic vibrations. We now note that the phase angle will remain constant as long as the variable $Z \equiv x \pm vt$ does so [19]. Any function $u(x,t)$ in which x and t appear only in the form $x \pm vt$ will satisfy Equation (2.4) and also the relation

$$\frac{\partial u}{\partial t} \pm v\left(\frac{\partial u}{\partial x}\right) = 0. \tag{2.8}$$

This shows that any disturbance of the string from its equilibrium shape may propagate along the string, with the entire waveform moving at velocity v and thus not distorting its shape over space and time. This property of non-dispersion is unique to Equation (2.4) and a system which obeys this equation is said to be non-dispersive. An example of a physical system that approximately obeys Equation (2.4) are longitudinal disturbances of a gas within a cylinder (an example of an acoustic wave) [19].

2.2.2 Dispersive Waves

Non-dispersive waves are very special however. Returning to our example of a string, when we described this system as non-dispersive we assumed that the string was perfectly flexible, *i.e.* that the only transverse force was due to tension. However, real strings are 'stiff', in that they tend to straighten

themselves even in the absence of tension. This additional force adds a higher order term to Equation (2.4) and makes the system dispersive. By considering the forces acting on a stiff string, we write the following equation [19]

$$\frac{\partial^2 u}{\partial t^2} = v^2 \left(\frac{\partial^2 u}{\partial x^2} - \alpha \frac{\partial^4 u}{\partial x^4} \right), \tag{2.9}$$

where α is a positive constant dependent on the shape of the cross-section and the elasticity of the string. We compare this to the non-dispersive wave equation (2.4) and note the additional higher order term. We wish to know whether such a system can still support the propagation of a travelling wave and so we substitute the expression (2.6) for a sinusoidal travelling wave into Equation (2.9) and find that ω and q must satisfy the following dispersion relation

$$\omega = \pm vq(1 + \alpha q^2)^{1/2}. \tag{2.10}$$

For a perfectly flexible string (*i.e.* $\alpha = 0$), this relation reduces to $\omega = vq$ which is the dispersion relation for the non-dispersive systems we previously described. For a slightly stiff string with a wavelength that is not too small, $\alpha q^2 \ll 1$ and we can write Equation (2.10) in the approximate form $\omega \approx \pm vq(1 + \frac{1}{2}\alpha q^2)$. We rewrite this expression as $\omega = cq - dq^3$, which is an expression for the dispersion relation of a slightly dispersive system. Substituting the equation for a sinusoidal travelling wave into this dispersion relation, we can convert Equation (2.9) into

$$\frac{\partial u}{\partial t} + v \left(\frac{\partial u}{\partial x} \right) + d \left(\frac{\partial^3 u}{\partial x^3} \right) = 0. \tag{2.11}$$

This is an example of a travelling wave equation for a slightly dispersive system. We may use the dispersion relation (2.10) to determine the phase velocity v_ϕ as we did for non-dispersive systems (see Equation (2.7)). For the dispersive system we are considering, v_ϕ is given by

$$|v_\phi| = v(1 + \alpha q^2)^{1/2}. \tag{2.12}$$

We note that the phase velocity depends on q. Thus, a travelling wave group composed of a superposition of sinusoidal waves will not retain its shape as it

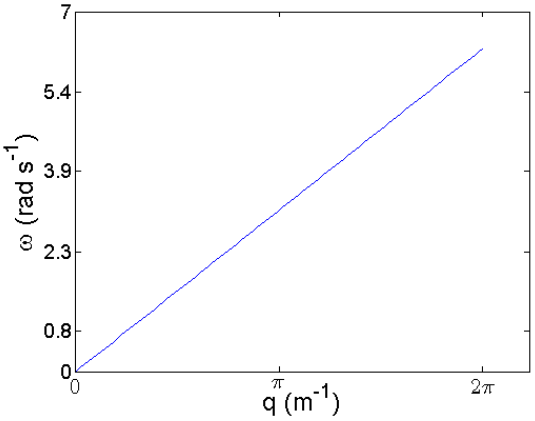

Figure 2.1: The dispersion relation for a non-dispersive system, with $\omega = vq$ and where we have assigned $v = 1$.

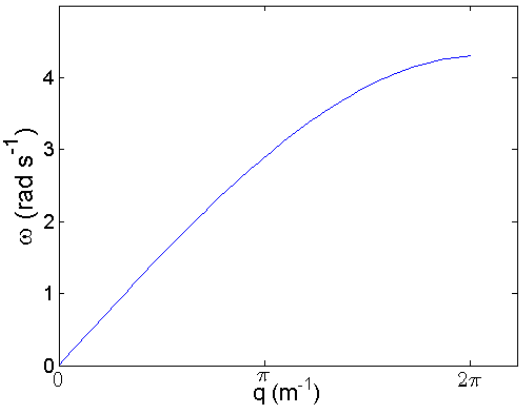

Figure 2.2: The dispersion relation for a slightly dispersive system, with $\omega = cq - dq^3$, where $c = 1$ and $d = 0.008$.

moves through a dispersive medium. This is due to the different components of the wave group moving at different velocities and is characteristic of a dispersive system. In the following section we will show how dispersion can combine with nonlinearity to allow a wave to propagate without a distortion in shape, *i.e.* a solitary wave.

2.3 A Balance of Nonlinearity and Dispersion

In nonlinear systems, the return force is not directly proportional to the displacement, as expressed by Equation (2.3). The characteristic speed of a wave is determined by the stiffness and the mass of the material through which it is travelling, so for a nonlinear system the speed will vary with the displacement $u(x,t)$. An example of an expression for the so-called *local speed*, v_l, in a nonlinear wave is [19]

$$v_l = v_0(1 + bu), \tag{2.13}$$

where v_0 is the wave speed at equilibrium (*i.e.* at $u = 0$) and b is a constant which depends on the particular properties of the system. The local speed v_l is the absolute speed with which a particular point in the wave signal travels through space. It differs from the wave speed which defines the speed relative to the medium. Local speed is easily understood in the context

of longitudinal waves where the medium moves back and forth along the direction of propagation with an instantaneous speed $\dot{u}$. If we denote the wave speed as c then the local velocity can be written as $v_l = c+\dot{u}$. Assuming the dispersion is negligible, the derivative $\dot{u}$ is in phase with the displacement u which leads to the approximate form of v_l given by Equation (2.13).

As described previously in the case of a linear system, in order for a signal to travel undistorted in the positive x direction the displacement $u(x,t)$ must be a function of $vt-x$ and must satisfy Equation (2.8). For a nonlinear system with a wave velocity which varies as in Equation (2.13), the following holds:

$$\frac{\partial u}{\partial t} + v_0(1+bu)\frac{\partial u}{\partial x} = 0. \tag{2.14}$$

Neglecting dispersion, nonlinearity causes a signal to be distorted as it moves through the material. If we add dispersion to the system, it might seem reasonable to assume that a material which is both dispersive and nonlinear is likely to distort the shape of a signal. However, dispersion and nonlinearity can sometimes cancel each other out, allowing a stable waveform to propagate indefinitely. We return to Equation (2.11), the wave equation for a slightly dispersive system, and substitute in Equation (2.14) containing the nonlinear term. This gives us the following wave equation which approximately describes the propagation of a wave in a slightly nonlinear and slightly dispersive material

$$\frac{\partial u}{\partial t} + v_0(1+bu)\frac{\partial u}{\partial x} + d\left(\frac{\partial^3 u}{\partial x^3}\right) = 0. \tag{2.15}$$

The equation above is in fact an expression of the KdV equation, initially introduced in Chapter 1 (see Equation (1.1)). This equation may be solved by a particular type of travelling wave, a solitary wave.

As shown previously, for a waveform $u(x,t)$ to propagate without any distortion of its shape, u must be a function of the variable Z. Using Z, we transform Equation (2.15) from a partial differential equation (PDE) to an ordinary differential equation (ODE), yielding

$$(v-v_0)u' - bv_0uu' - du''' = 0, \qquad u' \equiv \frac{\mathrm{d}u}{\mathrm{d}Z}. \tag{2.16}$$

Directly integrating this equation twice gives

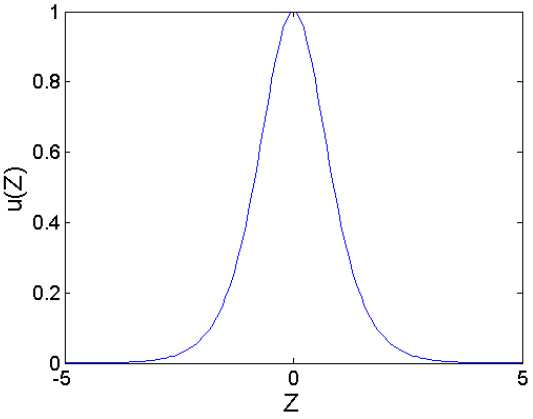

Figure 2.3: A plot of Equation (2.17) which is a solitary wave solution. We have set the constants β and γ equal to one.

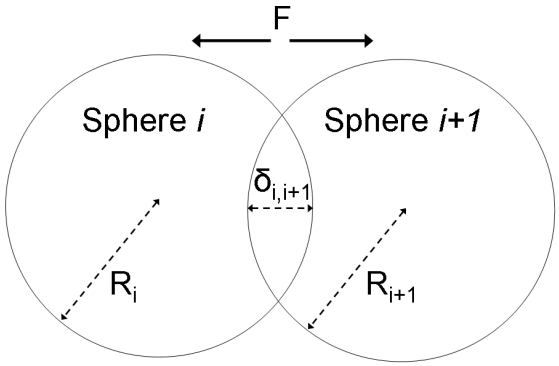

Figure 2.4: A schematic diagram showing two neighbouring spheres under compression. The spheres repel each other via the Hertz force F, where $F \propto \delta_{i,i+1}^{3/2}$.

$$\frac{1}{2}(v - v_0)u^2 - \frac{1}{6}bv_0u^3 - \frac{1}{2}du'^2 + Cu + D = 0,$$

where C and D are constants of integration. Assuming that our solitary wave solution is localised, we require $C = D = 0$ to ensure that u, $u' \to 0$ as $Z \to \pm\infty$. We can now rewrite the equation as

$$du'^2 = (v - v_0 - \frac{1}{3}bv_0u)u^2.$$

The equation may be simplified to

$$(u')^2 = (A - Bu)u^2$$

where $A = (v - v_0)/d$ and $B = bv_0/3d$. This ODE has the solution

$$u = \beta\,\mathrm{sech}^2(\gamma Z) \tag{2.17}$$

where $\beta = A/B$ and $\gamma = \frac{1}{2}A^{1/2}$. This is the solitary wave solution and is plotted in Figure 2.3. Using the condition for a maximum (*i.e.* $u' = 0$) we can also deduce the wave speed $v = v_0(1+\frac{1}{3}bu_{\max})$. Equation (2.17) gives us a simple qualitative understanding of the effect of dispersion and nonlinearity on our solitary wave: The more dispersive the medium (*i.e* larger d) the

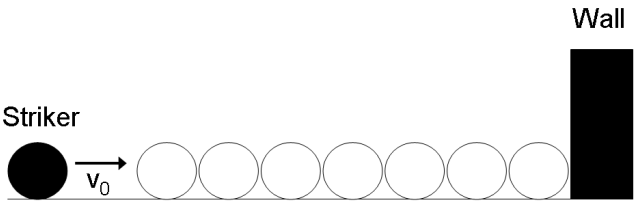

Figure 2.5: A 1D chain of spheres with an immovable wall at one end. The spheres interact on compression via the nonlinear Hertz force. The system may be set up in various ways. Two common initial conditions (ICs) are the "zero loading" case where the spheres are barely touching one another, and the precompressed state where there is overlap between the spheres possibly due to the chain being clamped.

broader the pulse; the greater the degree of nonlinearity (*i.e.* larger b) the narrower the pulse [19].

2.4 Hertzian Chains

2.4.1 The Hertz Force

The system investigated in this dissertation consists of a one dimensional chain of deformable spheres, shown schematically in Figure 2.5. We outline the properties of these chains before showing how solitary waves are obtained as approximate solutions to the equations of motion.

One of the key features of this system (along with asymmetry) is that the interaction force between the spheres, the Hertz force, is nonlinear. This repulsive force between two adjacent spheres under compression is expressed as

$$F = k\delta^{3/2}, \tag{2.18}$$

where the stiffness constant k can be expressed as a function of the properties of the interacting spheres and δ is the overlap between neighbouring spheres

(see Figure 2.4) [27]. Expressing this more formally, consider two spheres in contact, labelled i and $i+1$. These bodies have radii R_i and R_{i+1}, Young's moduli E_i and E_{i+1}, and Poisson ratios ν_i and ν_{i+1} respectively. Young's modulus E is a constant for a given material. It is used to express the relationship between stress σ and strain ϵ in a body via Hooke's Law: $\sigma = E\epsilon$. Poisson's ratio can be understood by considering a bar that is loaded in tension along its axis. There is lateral contraction ϵ_x (*i.e.* the bar becomes 'thinner') in addition to axial elongation ϵ_z (*i.e* the bar becomes longer). The Poisson ratio is defined as $\nu = -(\epsilon_x/\epsilon_z)$.

When the spheres are barely touching, the distance between the centres is given by $R_i + R_{i+1}$. Under compression, the spheres overlap by a distance defined by $\delta_{i,i+1} \equiv R_i + R_{i+1} - (u_i - u_{i+1})$, where u_i is the absolute position of sphere i. The potential energy associated with this compression is given by the Hertz potential

$$V(\delta_{i,i+1}) = \frac{2}{5D_{i,i+1}}\sqrt{\frac{R_i R_{i+1}}{R_i + R_{i+1}}}\delta_{i,i+1}^{5/2} \equiv a_{i,i+1}\delta_{i,i+1}^{5/2}, \tag{2.19}$$

where

$$D_{i,i+1} = \frac{3}{4}\left(\frac{1-\nu_i^2}{E_i} + \frac{1-\nu_{i+1}^2}{E_{i+1}}\right).$$

The following derivation of this Hertz potential (from Sen *et al.* [27]) is informal, though more detailed versions are also available [17, 18].

First, we wish to find an expression for the pressure between two identical spheres of radius R, with Young's modulus E and with a shared contact area proportional to $\tilde{r}^2$, where $\tilde{r}$ is the radius of the contact area. We define

$$r \propto \frac{\delta}{\tilde{r}}$$

as a measure of the deformation. Thus the pressure P experienced by the sphere is

$$P = Er = \frac{F}{\tilde{r}^2}$$

where F is the Hertz force between the spheres. From a purely geometrical argument we can also state

$$\tilde{r}^2 \propto \delta R$$

Combining the above expressions, we find that

$$E\left(\frac{\delta}{\tilde{r}}\right) \propto \frac{F}{\delta R} \Rightarrow E\left(\frac{\delta}{R}\right)^{1/2} \propto \frac{F}{\delta R}.$$

Thus,

$$F \propto ER^{1/2}\delta^{3/2}.$$

We note the force is proportional to $\delta^{3/2}$, which is characteristic of the Hertz law. Force is related to potential via the relation $F = -\mathrm{d}V/\mathrm{d}\delta$, so

$$V_{\mathrm{Hertz}}(\delta) \propto ER^{1/2}\delta^{5/2}.$$

In contrast, the linear return force described by Hooke's law has a potential which is quadratic in δ, $V_{\mathrm{Hooke}}(\delta) \propto \delta^2$. As shown in Figures 2.6 and 2.7, this results in the Hertz force being weaker than the Hooke force for small overlaps, and stronger for larger overlaps.

The Hertz law described above is a static law. However, we will be applying it to a dynamic system and thus must consider the following restrictions [22]:

1. The maximum shear stresses experienced by an individual sphere must be less than the elastic limit.

2. The sizes of the contact surfaces are much smaller than the radii of curvature of the particles.

In this model, we also neglect restitutive losses. This dissipation of energy in the system is due to the molecular nature of the interacting spheres - not all of the energy in the solitary wave will be transmitted due to part of it being absorbed by molecules in the spheres. This causes amplitude attenuation of the wave. There is currently no clear consensus on how best to incorporate these losses into the system models, with various dissipative terms being proposed [1]. For a discussion of these losses, see Ref.[1] and Section 4 of Ref.[27].

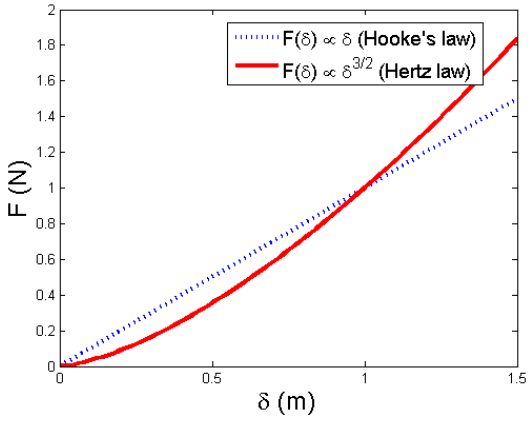

Figure 2.6: This plot shows a comparison of $F(\delta)$ for Hooke's law and Hertz's law. We see that for small δ, $F_{\text{Hooke}} > F_{\text{Hertz}}$ but the opposite is true at larger δ.

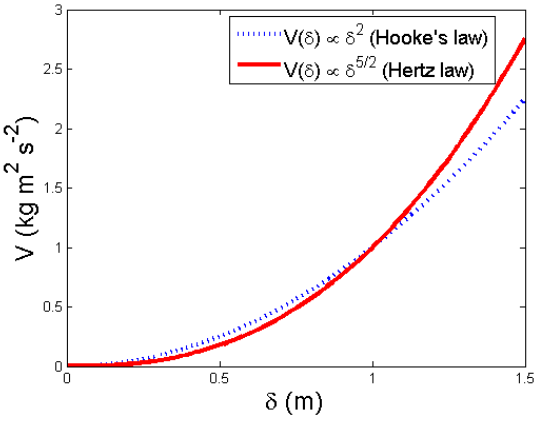

Figure 2.7: $V(\delta)$ for the Hooke and Hertz potentials. For lower δ, the Hooke system contains more potential energy but this is reversed for higher values of δ.

2.4.2 Equations of Motion and the Solitary Wave Solution

We now use the Hertz force to model the dynamics of our 1D granular lattice. A system of N identical interacting spheres can be described with a set of coupled nonlinear equations. We can write down the equation of motion for the i^{th} sphere as

$$m_i \ddot{u}_i = A_{i-1,i}(\Delta + u_{i-1} - u_i)_+^{3/2} - A_{i,i+1}(\Delta + u_i - u_{i+1})_+^{3/2}, \tag{2.20}$$

where $A_{i,i+1} \equiv (5/2)a_{i,i+1}$, Δ arises due to an initial precompression, and the index $+$ indicates that the Hertz force is zero when the spheres are not in contact [27]. An approximate solution to this system was first obtained by Nesterenko [23]. Here we present a version of this solution used initially by Chatterjee [2].

First, we are considering a chain of identical spheres so the force constants $A_{i,i+1}$ are the same for $1 \leq i \leq N-1$. We denote this value k. The masses are also identical so $m_i \equiv m$, $1 \leq i \leq N$. We are also going to assume there is no precompression (*i.e.* the "zero loading" case) and thus $\Delta = 0$. Systems such as this, where there is no linear force term, are known as "strongly nonlinear". We can now rewrite Equation (2.20) as

$$\ddot{\hat{u}}_i = (\hat{u}_{i-1} - \hat{u}_{i-1})^{3/2} - (\hat{u}_i - \hat{u}_{i+1})^{3/2}, \qquad 1 < i < N \tag{2.21}$$

where $\hat{u}_i(t) \equiv (k/m)^2 u_i(t)$. In order to establish our solution, we assume that when the chain of spheres is perturbed, this disturbance travels as a solitary wave. Thus, the displacement of each sphere can be described by the same function, albeit one which must be calculated at different times as the wave moves through the chain. By this consideration, we can write

$$\hat{u}_i(t) = \hat{u}_{i+1}(t + b), \tag{2.22}$$

where $b > 0$ is a constant. Using Equation (2.22) and choosing an arbitrary sphere as a reference, we can rewrite Equation (2.21) in terms of the displacement of this sphere as

$$\ddot{\hat{u}} = [\hat{u}(t + b) - \hat{u}(t)]^{3/2} - [\hat{u}(t) - \hat{u}(t - b)]^{3/2}. \tag{2.23}$$

Performing a power series expansion of $\hat{u}(t + b)$, we obtain

$$\hat{u}(t + b) = \hat{u}(t) + b\frac{\mathrm{d}\hat{u}}{\mathrm{d}t} + \frac{b^2}{2!}\frac{\mathrm{d}^2\hat{u}}{\mathrm{d}t^2} + \ldots.$$

We note at this point that we may also formulate this approximate solution using a long-wavelength approximation, where it is assumed that the characteristic spatial size of the perturbation is much greater than the distance between spheres. This approach is taken by Nesterenko [23], Porter *et al.* [25], and others.

Substituting the above expression into Equation (2.23) and then expanding in powers of b we obtain

$$\begin{aligned}\frac{\mathrm{d}^2\hat{u}}{\mathrm{d}t^2} = {} & \frac{3}{2}b^{5/2}\sqrt{\frac{\mathrm{d}\hat{u}}{\mathrm{d}t}}\frac{\mathrm{d}^2\hat{u}}{\mathrm{d}t^2} + \frac{1}{8}b^{9/2}\sqrt{\frac{\mathrm{d}\hat{u}}{\mathrm{d}t}}\frac{\mathrm{d}^4\hat{u}}{\mathrm{d}t^4} \\ & + \frac{1}{8}b^{9/2}\frac{\mathrm{d}^2\hat{u}/\mathrm{d}t^2}{\sqrt{\mathrm{d}\hat{u}/\mathrm{d}t}} \\ & + \frac{1}{64}b^{9/2}\frac{(\mathrm{d}^2\hat{u}/\mathrm{d}t^2)^3}{(\mathrm{d}\hat{u}/\mathrm{d}t)^{3/2}} + O(b^{13/2}).\end{aligned} \tag{2.24}$$

We now truncate our series by ignoring terms of order $O(b^{13/2})$ and higher. We note that this is not mathematically rigorous, we are just attempting

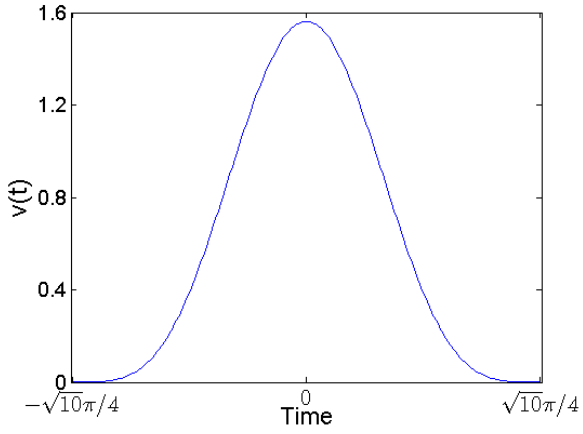

Figure 2.8: A temporal plot of the velocity of an arbitrary sphere in our 1D chain (Equation (2.26)).

to obtain an approximate solution that corresponds to experimental results [27]. Setting the parameter $b = 1$ this equation becomes

$$\begin{aligned}\frac{\mathrm{d}^2\hat{u}}{\mathrm{d}t^2} = \frac{3}{2}\sqrt{\frac{\mathrm{d}\hat{u}}{\mathrm{d}t}}\frac{\mathrm{d}^2\hat{u}}{\mathrm{d}t^2} + \frac{1}{8}\sqrt{\frac{\mathrm{d}\hat{u}}{\mathrm{d}t}}\frac{\mathrm{d}^4\hat{u}}{\mathrm{d}t^4} \\ + \frac{1}{8}\frac{\mathrm{d}^2\hat{u}/\mathrm{d}t^2}{\sqrt{\mathrm{d}\hat{u}/\mathrm{d}t}} \\ + \frac{1}{64}\frac{(\mathrm{d}^2\hat{u}/\mathrm{d}t^2)^3}{(\mathrm{d}\hat{u}/\mathrm{d}t)^{3/2}}.\end{aligned} \tag{2.25}$$

Equation (2.25) is satisfied by the expression [2]

$$v(t) = \frac{\mathrm{d}\hat{u}}{\mathrm{d}t} = \frac{25}{14}\cos^4\left(\frac{2t}{\sqrt{10}}\right), \qquad t \in (-\sqrt{10}\pi/4, \sqrt{10}\pi/4) \tag{2.26}$$

and outside this interval for t we set $v(t) \equiv 0$. Figure 2.8 shows a plot of this function.

A characteristic of nonlinear waves is that, unlike linear waves, the wave speed depends on the amplitude. This speed-amplitude relation can be found by a scaling analysis of the equation of motion for the ith sphere, *i.e.* [27]

$$m_i\ddot{u}_i = A_{i-1,i}(\Delta + u_{i-1} - u_i)_+^{3/2} - A_{i,i+1}(\Delta + u_i - u_{i+1})_+^{3/2}.$$

Using the estimates

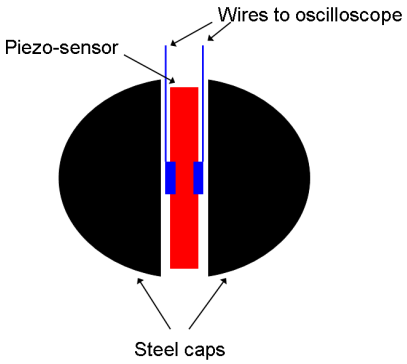

Figure 2.9: A schematic diagram of a sensor sphere used to measure force-time curves (adapted from [5]).

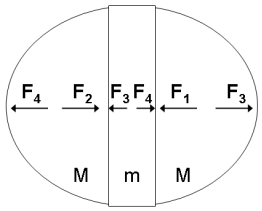

Figure 2.10: The forces acting on a sensor sphere under compression (also adapted from [5]).

$$\ddot{u}_i \sim \frac{L}{T^2}, \quad (\Delta + u_{i\pm1} - u_i)_+^{3/2} \sim L^{3/2}$$

where L and T are, respectively, the scaling parameters of displacement and time and assuming m_i and $A_{i-1,i}$ are fixed, we find

$$L \propto T^{-4}.$$

The impulse velocity v_i, which represents the solitary wave amplitude, scales as $v_i \propto L/T \propto T^{-5}$. The speed of the wave itself, v_s, has a scaling $v_s \propto 1/T$. Thus,

$$v_s \propto v_i^{1/5}.$$

For the Hertz force we know that $F_{\text{peak}} \propto \delta^{3/2}$ and so has the scaling $F_{\text{peak}} \propto L^{3/2}$. Combining these scaling relations gives us the speed-amplitude relation

$$v_s \propto F_{\text{peak}}^{1/6}. \tag{2.27}$$

This result is verified numerically in Section 2.6 (see Figure 2.14).

2.5 Experimental Setup

In addition to the extensive numerical simulations carried out on this Hertzian system [2, 12, 25] (simulations will be discussed in Section 2.6) there has also

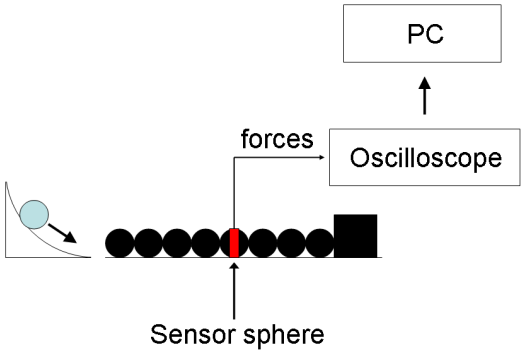

Figure 2.11: A schematic diagram of an experimental setup to investigate a 1D lattice with zero loading. The striker impacts the end of the chain with a velocity v_{init} sending a nonlinear wave propagating through the chain. The force at various points is measured using piezo-sensors embedded within spheres and is relayed to the oscilloscope. Figure adapted from Ref.[14].

been significant experimental work performed [15, 14, 25]. In this section we provide a brief account of the experimental methods used.

Figure 2.11 shows the setup for a zero loading experiment. Force-time measurements are made using piezo-sensors connected to oscilloscopes [25]. Whereas for numerical simulations a system consisting of hundreds of spheres may be investigated; experimentalists are restricted to using smaller chains. For instance, Job *et al.* use a maximum of fifty spheres [14] whilst Daraio *et al.* investigate chains of seventy to eighty spheres [25]. Experimental setups vary depending on the goals of the specific research, but it is typical to use sensors to measure the force versus time for several spheres in the lattice. The wave speed can also be obtained through "time-of-flight" measurements. One technique for incorporating the sensor into the system is to insert it into the middle of a sphere which has been sliced in half. It is important that the properties of this "sensor sphere", such as its mass and stiffness, are almost identical to those of the other spheres in the lattice. Figure 2.9 is a schematic diagram of a sensor sphere. In order to compare numerical and experimental studies of the system, it is important to relate the forces measured by the sensors to those calculated during simulations. This is described extensively by Daraio *et al.* [5] and the following discussions are based on those in that

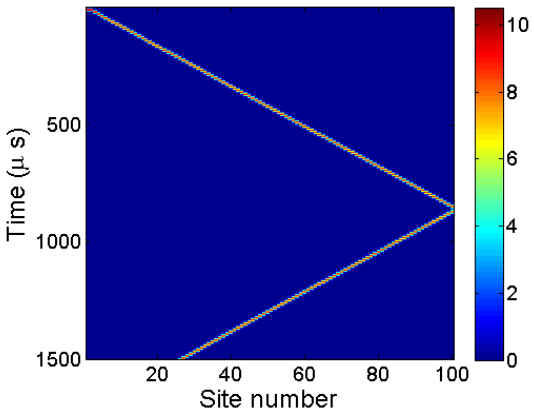

Figure 2.12: A spatiotemporal plot showing the propagation of a solitary wave through the lattice. The colour bar represents the force (in Newtons).

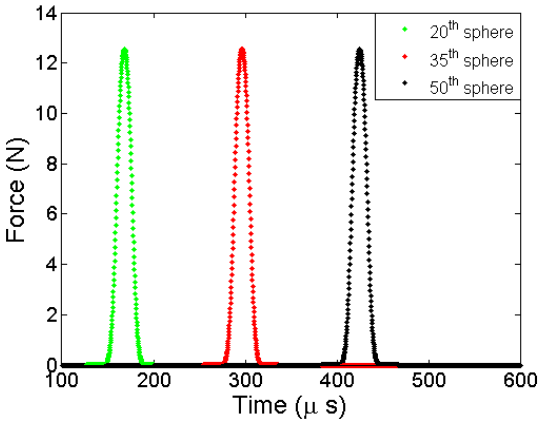

Figure 2.13: Force on three spheres in a uniform steel chain (each sphere has a radius of 0.0024 m). The striker was given an initial velocity of $0.443\,\mathrm{ms}^{-1}$.

paper.

Figure 2.10 shows the forces on a sensor sphere which is under compression. We can relate the forces acting on the sides of the sphere at the contacts with neighbouring spheres (F_1 and F_2) to those acting on the sides of the sensor (F_3 and F_4) via the equations [5]

$$F_3 = \frac{F_1 + F_2}{2} + \frac{F_1 - F_2}{2}\frac{m}{2M+m} \tag{2.28}$$

$$F_4 = \frac{F_1 + F_2}{2} - \frac{F_1 - F_2}{2}\frac{m}{2M+m}. \tag{2.29}$$

For the case of a light sensor $m \ll M$, where m is the mass of the sensor and M the mass of the cap, the forces on the sensor are very close to the average of the contact forces on the sphere *i.e.* $F_1 + F_2 \approx F_3 + F_4$. Thus we may assume that the forces measured numerically (F_1 and F_2) and those measured experimentally (F_3 and F_4) are equivalent.

2.6 Simulations and Results

Our system consists of $N+2$ particles with the $i = 0$ particle being a sphere that initially strikes the end of the chain (this is the striker) and the $i = N+1$ particle representing the wall. We consider a horizontal chain of spheres with zero loading *i.e.* initially the spheres are barely touching each other

($\delta_{i,i+1} = 0$, $1 \leq i \leq N$). The initial velocities v_i of the spheres $1 \leq i \leq N+1$ are set to zero. In order to instigate the propagation of a solitary wave in the chain, the striker is given an initial velocity. The wall at the end of the chain of spheres is modelled as an immovable sphere with infinite radius.

This system of coupled ODEs is solved numerically using a fourth-order Runge-Kutta (RK) finite difference scheme. Thus, our scheme is fourth-order accurate in time. For a more detailed discussion of the accuracy of this numerical solution see Appendix A of Ref.[2]. This RK method is implemented in the MATLAB code given in Appendix A. This code initialises the system and integrates forward in time. Figure 2.13 shows the numerical solution of our ODE system for $N = 100$, where the striker and all the spheres in the chain are made of steel (a uniform lattice). The properties of steel, and other materials, are given in Table 1. Figure 2.12 is a spatiotemporal plot of our uniform chain. In both figures, we can clearly observe a solitary wave propagate through the chain without dispersing, as predicted by the analysis in Section 2.4.2.

We also investigate numerically the speed-amplitude relation that was derived in Section 2.4.2. Equation (2.27) indicates that the wave speed v_s varies with force amplitude F_{peak} according to the $v_s \propto F_{\text{peak}}^{1/6}$. The results of numerical simulations, shown in Figure 2.14, confirm the accuracy of this relation. The wave speed is calculated using time-of-flight measurements.

Table 1: Properties of various materials used in simulations (values from Ref.[25]).

Material	$\rho(\text{kg m}^{-3})$	E (GPa)	ν
Steel	7780	193	0.3
PTFE	2178	1.46	0.46
Rubber	1383	0.03	0.49
Brass	8500	103	0.34

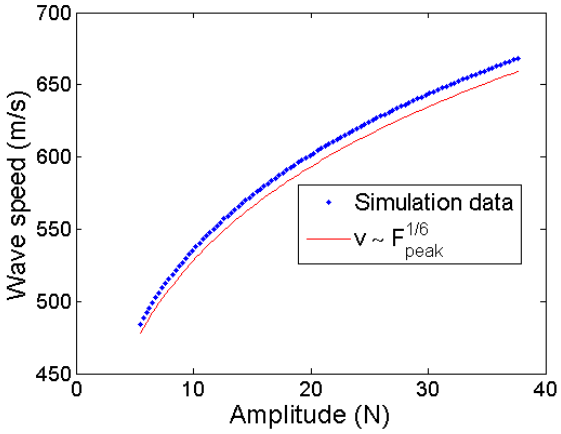

Figure 2.14: The scaling relation between solitary wave velocity and amplitude (expressed by Equation (2.27)) is verified by numerical simulations, with the results shown in this diagram.

3 Defects in Granular Lattices

3.1 Overview of Granular Defects

We showed in Chapter 2 how a 1D chain of spheres, interacting via a Hertzian potential, can display nonlinear localisation effects. For instance, a precompressed chain is dispersive and allows perturbations to propagate as weakly nonlinear acoustic waves. By contrast, in a chain where the spheres are barely touching one another an initial impulse will travel as a highly nonlinear solitary wave. As described in Section 2.3, this solitary wave solution arises due to a balance between nonlinearity and dispersion in the system.

These results apply to homogeneous chains of spheres *i.e.* those where the constituents all have identical size and material properties. However, most real systems will contain defects. Such a heterogeneity may unbalance the dispersion and nonlinearity of the system, breaking the solitary wave symmetry. This can be clearly seen in Figures 3.1 and 3.2. Various kinds of heterogeneities exist, affecting the propagating impulse in different ways. For example, a pulse travelling through a chain with decreasing sphere size will develop a long tail. This has the effect of extending the momentum transfer in time. A potential application of this phenomenon is in the design of impact protection systems [15]. Additionally, chains containing periodic

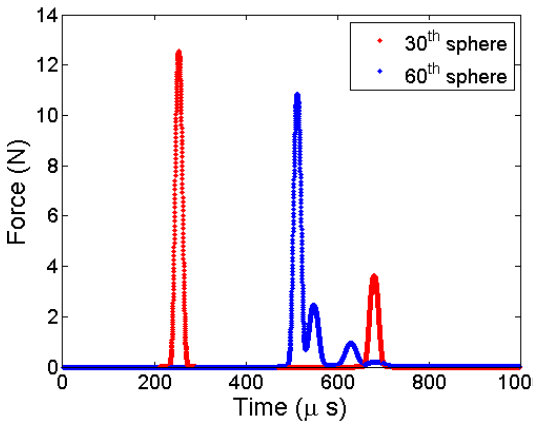

Figure 3.1: Force versus time for two spheres in a chain with $N = 100$. The defect is a steel sphere of radius $0.1R$ located at $i = 50$ in an otherwise homogeneous steel chain. The second red peak indicates reflection from the defect. We also observe that the solitary wave loses its symmetry after passing through the mass defect.

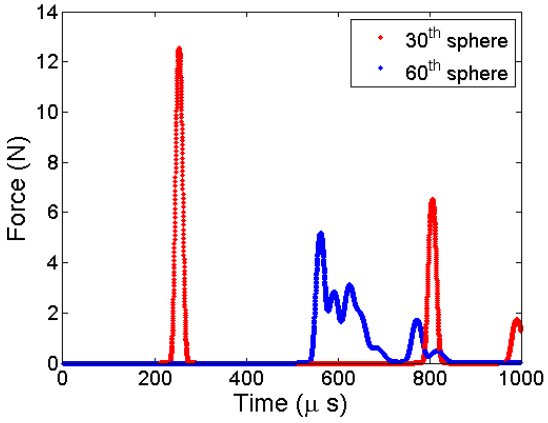

Figure 3.2: Here, the defect is made of polytetrafluoroethylene (PTFE) and is placed at $i = 50$ in an otherwise homogeneous steel chain. The properties of both these materials are given in Table 1. The radius matches that of the other spheres in the chain. Once again, we see partial reflection of the wave and a transmitted portion that has lost its symmetry.

arrangements of different masses, such as dimers and trimers, have been shown to support localised nonlinear waves [25].

There has been much interest in these systems due to the fact that the properties of granular lattices are tunable. In addition to including particles of various masses to the lattice, the behaviour of the system may also be controlled by the addition of different materials with specific material properties (*i.e* Young's modulus E, Poisson ratio ν, and density ρ). These properties alter the coefficients $A_{i,i+1}$ between spheres which are given by the formula

$$A_{i,i+1} = \frac{4E_iE_{i+1}}{3[(E_{i+1}(1-\nu_i^2) + E_i(1-\nu_{i+1}^2)]} \left(\frac{R_iR_{i+1}}{R_i + R_{i+1}}\right)^{1/2}.$$

The ability to tune the response of granular systems to perturbations has led to a plethora of potential applications including sound and shock absorbers, sound focusing devices, and scramblers [27]. In addition to tailoring the system's response for various industrial devices, it is also important to understand the basic interactions of nonlinear pulses with various defects.

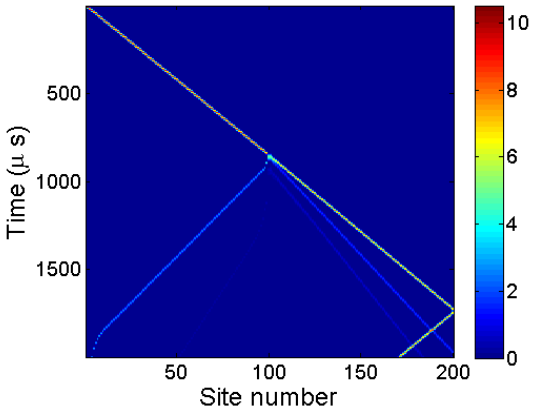

Figure 3.3: A spatio-temporal plot showing the propagation of a solitary wave through a lattice that contains a light defect located at site 100 ($R_{\text{defect}} = 0.1R_{\text{chain}}$, where R_{defect} is the defect radius and R_{chain} is the radius of the other spheres in the chain). We note the secondary waves that are created when the solitary wave interacts with the defect.

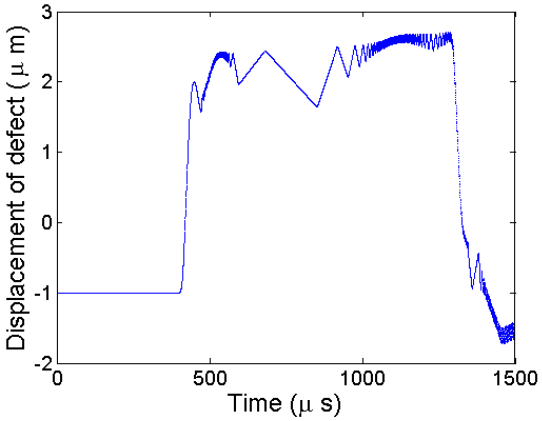

Figure 3.4: Plotted above is the displacement of the light defect in an otherwise homogeneous chain. We observe that the propagating solitary wave causes the defect to shift suddenly and then oscillate rapidly. These oscillations cause the defect to collide with neighbouring spheres, creating the secondary waves we see in Figure 3.3.

Such an understanding can enable us to probe the internal composition of solid objects in a nondestructive manner [13].

It is the impact of the size and material properties of defects on wave propagation in Hertzian lattices that is the primary focus of this chapter. We perform numerical simulations that probe the effect of different defects on the properties of the solitary wave that propagates through the chain. These results are presented below.

3.2 Results and Discussion

Initially we consider a steel defect of varying size in an otherwise homogeneous chain of steel spheres. The behaviour of the granular system is remarkably different depending on whether the impurity is larger or smaller than the other spheres in the chain. We now examine both these cases [12].

3.2.1 Light and Heavy Defects

As we just alluded to, a granular lattice with an embedded defect will show very different behaviour depending on the size of that defect. These differences manifest themselves as different patterns of scattered waves. Firstly we consider the effect of a light defect. By a light defect, we mean a sphere that is lighter than the others in the chain (but which has the same values of E and ν). Such a system is characterised by a backscattered solitary wave followed by a succession of so-called secondary waves with successively decreasing amplitudes. The source point of these secondary waves is the defect location. A portion of the initial impulse's energy is transmitted by the defect and this wave is also followed by secondary waves. These features can be seen in Figure 3.1. Figure 3.4 shows the displacement of the defect versus time. We see that the solitary wave propagating through the chain causes the defect to oscillate. These oscillations are damped due to the defect colliding with its nearest neighbours. It is these collisions that generate the secondary waves that propagate through the chain in both directions, with the light defect acting as a wave source. Figure 3.3, which is a spatio-temporal plot of the forces on the chain spheres, also illustrates the behaviour of the light defect. We observe the solitary wave travel through the lattice and encounter the defect located at site 100. As we have outlined, this causes oscillations of the defect, generating secondary waves of decreasing amplitude in both directions. By looking at the slopes of the travelling wave patterns, we see that these reduced-amplitude secondary waves travel at lower velocities than the initial impulse. This is a typical nonlinear phenomenon and one which we considered in Section 2.4.2. In that discussion, we used scaling analysis to find the relation $v_s \propto F_{\text{peak}}^{1/6}$ which was then verified numerically.

The interaction of a solitary wave with a heavy defect produces behaviour that is markedly different from that described above. Instead of exciting oscillations, the wave shifts the heavy defect in the direction of its propagation. This causes the lattice to be split in two, with pulses propagating in each part. Figure 3.5 shows this clearly. Beyond the defect we observe many pulses of decreasing amplitudes. In front, there is just a single pulse of large amplitude. The collision of the solitary wave with this heavy defect causes it to fragment into solitary waves of decreasing amplitudes.

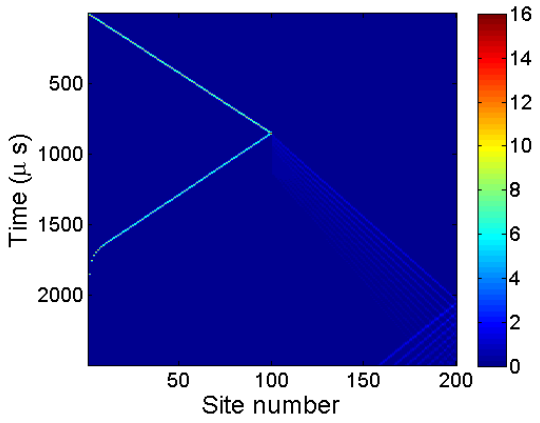

Figure 3.5: This is a spatio-temporal plot of a solitary wave propagating through a steel chain which contains a large defect at site number 100. The defect has $R_{\text{defect}} = 3R_{\text{chain}}$.

Figures 3.6, 3.7 and 3.8 show the effect of defect size on solitary wave amplitude, width and velocity respectively. In all these simulations, the defect has been placed in the middle of an otherwise homogeneous chain of steel spheres. The size of the defect is varied but the Young's modulus E and Poisson ratio ν remain constant. In Figure 3.6 we see that maximum transmission occurs when the defect is the same size as the other spheres in the chain *i.e.* the chain is homogeneous. Fragmentation of the solitary wave by the defect cuases its amplitude to be decreased. We also observe a secondary peak in the transmission curve below the primary peak at $R_{\text{defect}} = R_{\text{chain}}$. The origin of this additional peak is not clear and deserves further investigation. A similar peak, though less pronounced, is seen in Figure 3.7. This diagram shows that defects cause the propagating pulse to widen. The velocity of the solitary wave as a function of defect size is shown in Figure 3.8. The velocity is calculated by time-of-flight measurements between two fixed spheres, one on either side of the defect. Thus we are effectively measuring the average speed of the wave between these spheres. The velocity is a maximum for $R_{\text{defect}} = R_{\text{chain}}$. For $R_{\text{defect}} \neq R_{\text{chain}}$ there are secondary pulses produced which has the effect of reducing the solitary wave amplitude and consequently, because of the relation $v_s \propto F_{\text{peak}}^{1/6}$ (which has been verified for the uniform chain), its velocity.

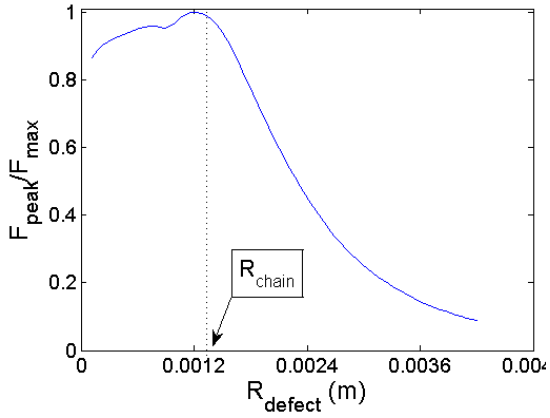

Figure 3.6: This plot shows the variation of transmitted solitary wave amplitude with defect radius, R_{defect}. The defect is inserted into a steel chain and has material properties identical to the other spheres. We note that there is complete transmission when R_{defect} matches the radii of the other spheres, R_{chain}.

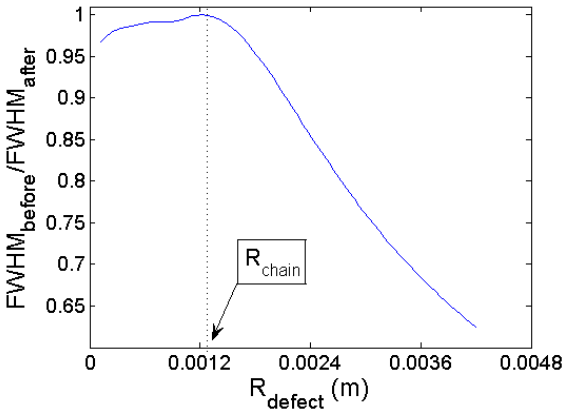

Figure 3.7: Here we see the variation of the full width at half maximum (FWHM) of the solitary wave with defect radius. This is a measure of the spatial extent of the pulse. The term $\text{FWHM}_{\text{before}}$ denotes the width before the interaction with the defect and $\text{FWHM}_{\text{after}}$ is the width after this interaction.

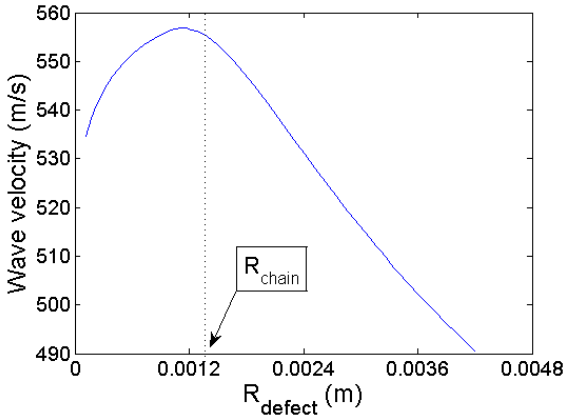

Figure 3.8: This diagram shows the dependence of the velocity of our solitary wave with R_{defect}. The velocity is calculated using time-of-flight-measurements and we see that the wave has its highest velocity when $R_{\text{defect}} = R_{\text{chain}}$.

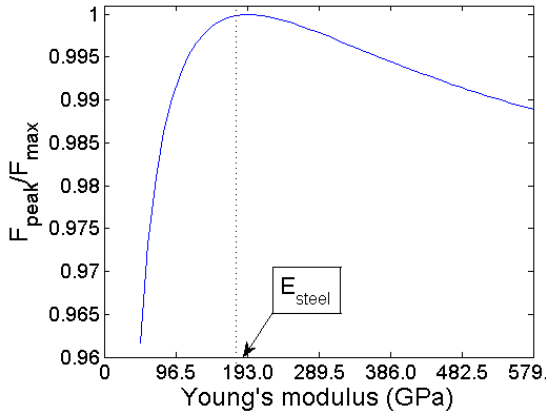

Figure 3.9: The variation of $F_{\text{peak}}/F_{\text{max}}$ with Young's modulus E is plotted above. The size and other properties of the defect are kept constant and equal those of the other spheres.

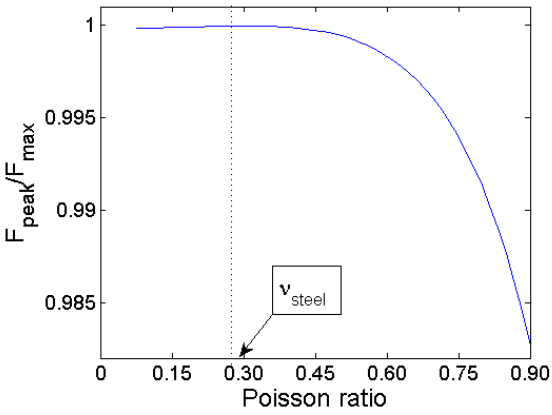

Figure 3.10: This time we vary the Poisson ratio ν and measure the transmitted amplitude of the incoming solitary wave. We again note that transmission is maximised for $\nu_{\text{defect}} = \nu_{\text{chain}}$.

3.2.2 The Effect of Young's Modulus E and Poisson Ratio ν

In the previous section we considered a defect to be a sphere of varying size, with all its other properties matching those of the chain. Now we consider the effect of holding the defect size constant and varying, in turn, the Young's modulus E and Poisson ratio ν. The results are plotted in Figures 3.9-3.14.

In Figures 3.9 and 3.10 the transmitted solitary wave amplitude is plotted as a function of E and ν respectively. Due to a material defect, the energy of the solitary wave is not conserved as it moves through the granular lattice. The interaction of the wave with the defect produces secondary waves that carry away some of the original solitary wave's energy [24]. It also causes the amplitude of the wave to be decreased, as seen in Figures 3.9 and 3.10. The variations are much smaller than those observed in Figure 3.6 indicating that the defect's mass is the predominant property when considering transmission.

The width of our solitary wave is measured both before and after interaction with the defect. The ratio $\text{FWHM}_{\text{before}}/\text{FWHM}_{\text{after}}$ is calculated for varying E and ν. We observe that the pulse broadens as these properties deviate from those of the other spheres in the chain.

Figures 3.13 and 3.14 show the variation of the wave velocity with E and ν respectively. As the defect becomes "stiffer", *i.e.* as E increases, the speed

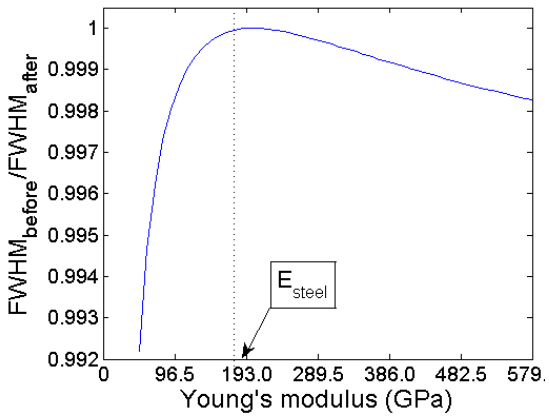

Figure 3.11: The FWHM of the propagating wave is measured as a function of E. The ratio $\text{FWHM}_{\text{before}}/\text{FWHM}_{\text{after}}$ is plotted here.

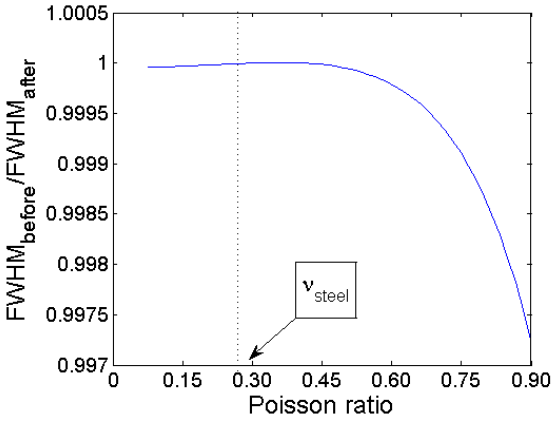

Figure 3.12: In this instance we vary the Poisson ratio of our defect in order to observe its effect on the width of the solitary wave.

increases. We can understand this qualitatively by considering that because the defect is not compressed to the same degree, it transfers the incoming energy more quickly [25]. Similar behaviour is observed for ν (see Figure 3.14). Recall that the formula for the Poisson ratio is $\nu = -\epsilon_x/\epsilon_z$, where ϵ_x is the lateral contraction and ϵ_z is the axial elongation. Increasing ν effectively means that ϵ_z is decreasing relative to ϵ_x, *i.e.* the sphere is compressed less. This leads to the solitary wave passing more quickly through the defect.

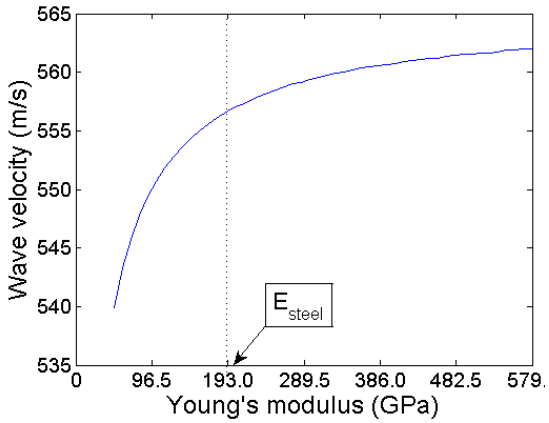

Figure 3.13: This plot shows the variation of wave velocity with E.

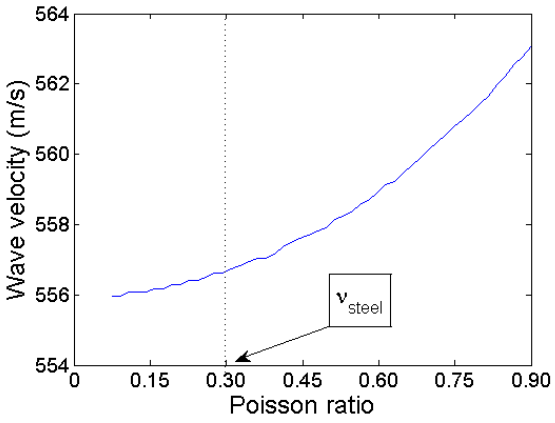

Figure 3.14: The effect of ν on the wave velocity is plotted here.

4 Wave Interactions with Discrete Breathers

4.1 Introduction

Investigations of FPU systems (previously described in Chapter 1) have shown how energy can be localised in a finite number of modes, despite interaction between all the modes in the system. Previous to these studies, it was presumed that such systems would eventually thermalise *i.e.* after a certain period of time the energy would be evenly distributed amongst all the modes [26]. Further to these observations, FPU systems have been shown to allow for solutions in which the energy is not localised in certain modes but rather it is localised in real space. In the context of the granular lattices being investigated here this means that the energy is not shared amongst all the spheres in the chain but rather it is shared by a subset of the constituents. Solutions of this form are known as *intrinsic localised modes* (ILMs), or *discrete breathers* (DBs). ILMs/DBs are time-periodic and spatially localized solutions that arise due to the interplay between nonlinearity and discreteness

4.2 The Phenomenon of Resonance

Resonance is an important phenomenon that appears in various guises throughout physics. One form of resonance is the response of a system to an external

excitation at a certain frequency [20]. An example is the response of a lightly damped harmonic oscillator to a periodic force (see Figures 4.1 and 4.2). We consider the harmonic driving force with angular frequency Ω to have the form

$$F(t) = F_0 \cos \Omega t,$$

where F_0 is the amplitude of the driving force. The equation of motion of the oscillator can then be described by

$$m\ddot{\psi} = -k\psi - b\dot{\psi} + F_0 \cos \Omega t$$

where ψ is the displacement of the oscillator, m is the mass, k is the usual force constant and b is a resistance term due to the damping. Dividing through by m gives the usual form of this ODE

$$\ddot{\psi} = -\Omega_0^2 \psi - \gamma\dot{\psi} + (F_0/m) \cos \Omega t. \tag{4.1}$$

Here we have defined $\Omega_0^2 \equiv k/m$ and $\gamma \equiv b/m$. The quantity Ω_0 is simply the angular frequency of the free, undamped oscillator. After a period of time, we expect the system to reach a steady state in which the mass m is vibrating harmonically at the same frequency as the driving force. In light of this assumption, we say that the displacement of our oscillator is given by

$$\psi = A(\Omega) \cos(\omega t + \phi),$$

where $A(\Omega)$ is a frequency-dependent amplitude and ϕ is the phase constant. The dependence of A on Ω gives rise to resonance in the system. It may be shown that

$$A = \frac{F_0}{m} \left(\frac{1}{(\Omega_0^2 - \Omega^2)^2 + \gamma^2 \Omega^2} \right)^{1/2}. \tag{4.2}$$

Equation (4.2) is plotted in Figure 4.2. We clearly see that A reaches a maximum for $\Omega \approx \Omega_0$ and we thus define $\nu_0 \equiv \Omega_0/2\pi$ to be the *resonance frequency* [19].

We extend this discussion to a system comprising of a driven oscillator coupled to another oscillator. In such a setup, there are two resonant frequencies corresponding to the fundamental frequencies Ω_1 and Ω_2 of each

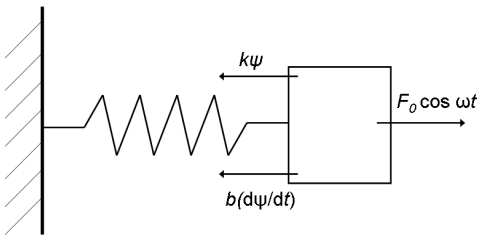

Figure 4.1: This diagram shows the forces acting on a lightly damped, driven oscillator. The driving force is periodic in time and has the form $F(t) = F_0 \cos(\Omega t)$. $k\psi$ is the usual return force, and $b\dot{\psi}$ is a resistance force.

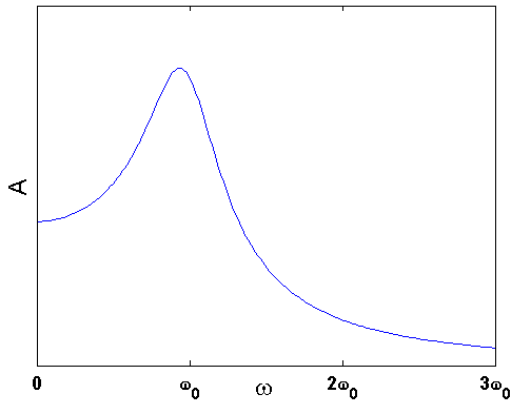

Figure 4.2: This is an example of a response curve for a lightly damped oscillator. We see that the amplitude A of the driven mass is a maximum for $\Omega \approx \Omega_0$. $\nu_0 = \Omega_0/2\pi$ is known as the resonance frequency for the system.

oscillator. The forced oscillator experiences the usual resonance (as just described) for $\Omega = \Omega_1$. This resonance is characterised by a symmetric profile and is described by a Lorentzian function[2]. However, for $\Omega = \Omega_2$, *i.e.* at the resonant frequency of the oscillator to which it is coupled, there is a second resonance which is characterised by an asymmetric profile [20]. This is a Fano resonance and was explained by Ugo Fano in his celebrated paper of 1961 [6]. Recently, Fano resonances have been predicted for weakly nonlinear systems such as nonlinear waveguide arrays and in Bose-Einstein condensates [21]. We investigate the possibility of observing analogs of Fano resonances in our highly nonlinear system, the Hertzian lattice. We now discuss Fano resonance in greater detail.

4.3 Fano Resonance

As mentioned previously, Fano resonances are characterised by an asymmetric profile. Fano explained the origin of these "strange looking shapes" in

[2]The Lorentzian function (also known as the Cauchy-Lorentz distribution) is given by $f(x) = \frac{1}{\pi}\left[\frac{\gamma}{(x-x_0)^2+\gamma^2}\right]$. The parameter x_0 defines the position of the curve and γ defines its width.

terms of the interaction of a localised state with a continuum of propagation modes. His description was initially introduced to explain sharp, asymmetric profiles in atomic absorption spectra which had been observed by Beutler [20]. Fano hypothesised that the unexpected profiles arose due to the interaction of a discrete excited state of an atom with a continuum which shared the same energy. The interaction results in interference and the observed profiles.

A qualitative understanding of these novel resonances was provided by Fano in terms of the absorption of radiation by atoms. We now present an account of this explanation based on the description given in Ref. [20]. Quantum theory tells us that electrons in atoms may only have certain energy values *i.e.* the energy spectrum is discrete rather than continuous. Electrons may move between different energy levels by absorbing or emitting packets of radiation called *photons*. The energy of a photon is given by $E_{photon} = \hbar\omega$. If $E_{photon} = E_2 - E_1$, where E_1 and E_2 are the energies of levels 1 and 2 respectively, then an electron may move between these levels by absorbing or emitting a photon of this frequency. Thus if we shine light of varying frequency on a sample of atoms, there will be absorption resonance curves at values of ω corresponding to various energy gaps. These absorption peaks are symmetric and may be represented using the Lorentzian function defined in the previous section.

However, a different situation can arise whereby absorption of radiation occurs via a different mechanism. The *Auger effect* describes how an electron from the inner core of an atom can be removed by high energy radiation (such as an X-ray) leaving a vacancy in the core. An electron from a higher energy level may relax into this "electron hole" resulting in a release of energy. Sometimes this energy can be emitted in the form of a photon but often it is transferred to another electron which is above the ionisation threshold and this electron will escape from the atom. Due to the superposition principle, the Auger effect can interfere with the normal relaxation processes in an atom and this manifests itself as an asymmetric peak in the spectra of that atom (Fano resonance).

An important concept in the understanding of Fano resonance (and of wave scattering in general) is that of "channels". In an atom, an excited

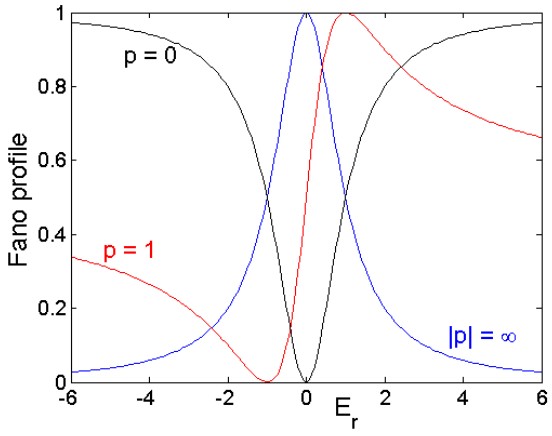

Figure 4.3: Various resonance profiles plotted using Equation (4.3) for various values of p. Adapted from Ref.[20].

state consists of an electron in a higher energy level (referred to as a bound state in one sub-band) co-existing with an electron hole in a lower level (an unbound state in another sub-band). In atomic physics, one can think of separate sub-bands as channels. This is a useful way to formulate our system, as it allows us to explain Fano resonances in terms of interference between various scattering channels.

Although Fano's original explanation was applied to atomic spectra, the great strength of his theory is that it can be generalised to describe asymmetric profiles in terms of interference, regardless of the nature of the particular system. Fano wrote down a formula for the shape of the resonance curve which has since been used to interpret a variety of experimental data

$$\sigma = \frac{(E_\mathrm{r} + p)^2}{E_\mathrm{r}^2 + 1}. \tag{4.3}$$

Here, p is a shape parameter and E_r is a reduced energy. For $|p| \to \infty$, Equation (4.3) describes a Lorentzian curve and for $p = 0$ it gives an inverted Lorentzian. For $0 < p < \infty$ the profile is asymmetric, as we expect for Fano resonance (see Figure 4.3).

We will now introduce a model for Fano resonance, known as the Fano-Anderson Model, which we use to derive a formula for the transmission coefficient which has the form of the equation originally written down by Fano (4.3).

4.3.1 The Fano-Anderson Model

A relatively simple model that can be often invoked to explain the physics of Fano resonance is the Fano-Anderson model. This is a discrete model which can be described by the following Hamiltonian [20]

$$H = \sum_n C\phi_n\phi_{n-1}^* + E_F|\psi|^2 + V_F\psi^*\phi_0 + \text{complex conjugates}, \tag{4.4}$$

where the asterisk denotes the complex conjugate and H describes the energy of two subsystems. The first is a linear discrete chain with field amplitude ϕ_n at site n. The symbol C denotes the coupling constant between neighbouring sites. This system allows the propagation of plane waves with the dispersion relation $\omega_q = 2C\cos q$. The state of the second subsystem is denoted ψ and has an energy value E_F, where E_F denotes the Fermi energy. The interaction between the subsystems is described by the coupling term V_F from the state ψ to site 0 of the discrete chain, ϕ_0. Using Equation (4.4) the following dynamical equations can be obtained:

$$\begin{aligned} \mathrm{i}\dot{\phi}_n &= C(\phi_{n-1} + \phi_{n+1}) + V_F\psi\delta_{n0} \\ \mathrm{i}\dot{\psi} &= E_F\psi + V_F\phi_0 \end{aligned} \tag{4.5}$$

where δ_{n0} denotes the Kronecker delta. Due to the gauge invariance of these equation, the time dependence can be removed using the ansatz

$$\begin{aligned} \phi_n(t) &= A_n\mathrm{e}^{-\mathrm{i}\omega t}, \\ \psi_n(t) &= B\mathrm{e}^{-\mathrm{i}\omega t}. \end{aligned} \tag{4.6}$$

These expressions inserted into Equations (4.5) give the following static equations

$$\begin{aligned} \omega A_n &= C(A_{n-1} + A_{n+1}) + V_F B\delta_{n0}, \\ \omega B &= E_F B + V_F A_0. \end{aligned} \tag{4.7}$$

Given the dispersion relation for the linear system, *i.e.* $\omega_q = 2C\cos q$, we should look to solve the above system of equations using frequencies from

the propagation band *i.e.* $\omega = \omega_q$. We are dealing with a wave scattering problem so we can impose the following boundary conditions on A_n:

$$A_n = \begin{cases} I_{\text{Fano}} e^{iqn} + r_{\text{Fano}} e^{-iqn}, & n < 0 \\ T_{\text{Fano}} e^{iqn}, & n > 0 \end{cases} \tag{4.8}$$

where I_{Fano}, r_{Fano} and T_{Fano} are the incoming, reflected and transmitted wave amplitudes respectively. We use the second equation in the system (4.7) to obtain

$$B = \frac{V_F A_0}{\omega_q - E_F}.$$

Our system (4.7) can now be reduced to

$$\omega_q A_n = C(A_{n-1} + A_{n+1}) + \frac{V_F^2}{\omega_q - E_F} A_0 \delta_{n0}. \tag{4.9}$$

Examining Equation (4.9), we see that the magnitude of the scattering potential $V_F^2/(\omega_q - E_F)$ is dependent on the plane wave frequency ω_q. This is important, as we note that for $\omega_q = E_F$, the scattering potential is infinite and prevents transmission of the incoming wave. This is a key feature of Fano resonance.

We can derive an expression for the transmission coefficient $T = |T_{\text{Fano}}/I_{\text{Fano}}|^2$ using a transfer matrix approach as described in Ref.[29]. First, write Equation (4.9) in the form of a transfer matrix

$$C \begin{pmatrix} A_{n+1} \\ A_n/C \end{pmatrix} = \mathbf{T_n} \begin{pmatrix} A_n \\ A_{n-1} \end{pmatrix} \tag{4.10}$$

with

$$\mathbf{T_n} = \begin{pmatrix} \omega_q - \frac{V_F^2}{\omega_q - E_F}\delta_{n0} & -C \\ 1 & 0 \end{pmatrix}. \tag{4.11}$$

If there are $n = N_{left}$ sites to the left of site $n = 0$ and $n = N_{right}$ sites to the right, then we can write

$$C \begin{pmatrix} A_{N_{right}} \\ A_{N_{right}-1}/C \end{pmatrix} = \mathbf{P_{N_{right}}} \begin{pmatrix} A_{-N_{left}+1} \\ A_{-N_{left}} \end{pmatrix} \tag{4.12}$$

where

$$\mathbf{P_{N_{right}}} = T_{N_{right}} T_{N_{right}-1} \cdots T_1 T_0 T_{-1} \cdots T_{-N_{left}}.$$

Using Equations (4.8) and (4.12) an expression for T may be derived. This is given in Ref.[20] as

$$T = \frac{\alpha_q^2}{\alpha_q^2 + 1}, \tag{4.13}$$

where

$$\alpha_q = c_q(E_F - \omega_q)/V_F^2, \quad c_q = 2C \sin q.$$

We note that Equation 4.13 corresponds to the formula introduced by Fano (Equation (4.3)) to explain the unusual atomic absorption lines observed by Beutler. Transmission vanishes for $\omega_q = E_F$.

These discussions have shown the possibility of waves travelling through a the linear chain interacting with those in the discrete state leading to Fano resonance.

4.4 Discrete Breathers

As we have discussed in previous chapters, nonlinear lattices can support the propagation of weakly and strongly nonlinear waves. These are solutions to the equations of motion of the system, which are characterised by Hertzian interactions between neighbouring spheres. Another family of solutions are DBs, which are spatially localised and often time periodic excitations of the lattice. In this chapter, we consider DBs in a precompressed chain. Snapshots of an oscillating DB are shown in Figure 4.4. DBs are similar to solitary waves with the added property of being periodic in time. They arise due to the interplay of nonlinearity and discreteness in the system. Nonlinearity indicates that the DB amplitude and localisation length are dependent on the frequency of oscillation, Ω_b, and can therefore be tuned. Discreteness means that there is an upper bound, ω_q, on the frequency spectrum of the waves that can propagate through the chain [9].

The phenomenon of localised modes, and DBs in particular, is quite widespread and such states have been experimentally observed in fields as diverse as nonlinear optics, Josephson junctions, magnetic systems, and in the lattice dynamics of crystals [9].

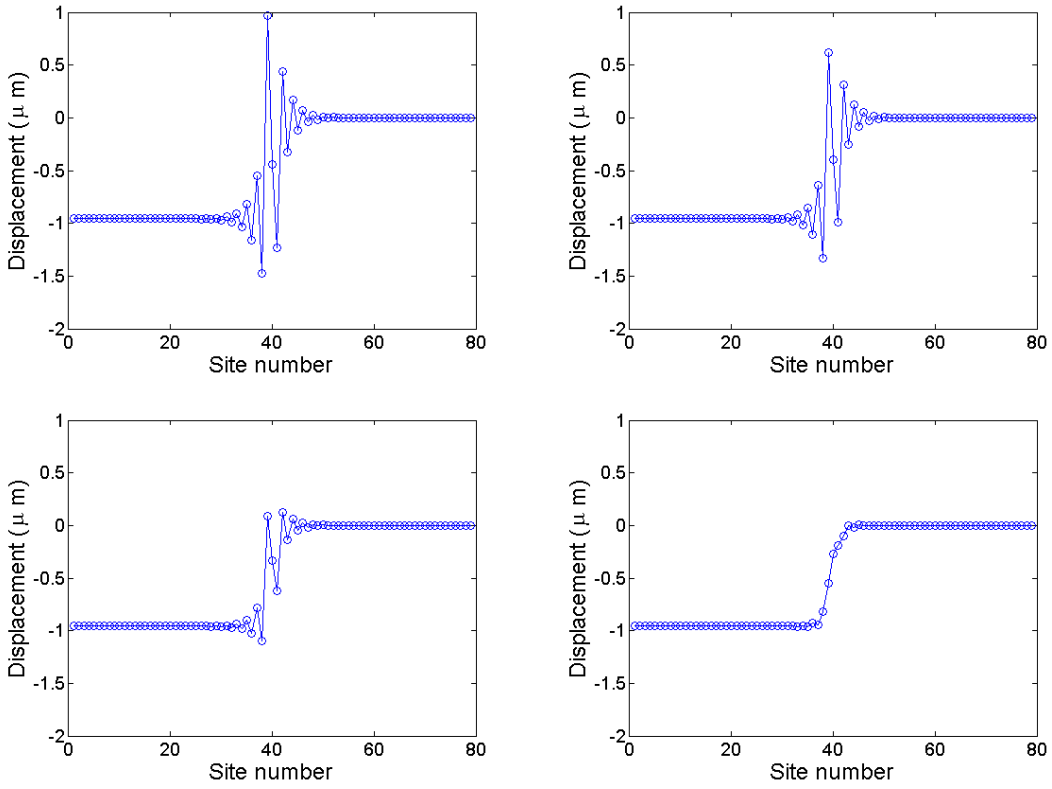

Figure 4.4: Snapshots of an oscillating discrete breather at various times. We note the spatial localisation of this mode. This DB has a frequency of 21300 Hz and was originally used by Theocharis *et al.* [28].

We begin a more quantitative description of DBs by considering the total energy of our precompressed granular lattice *i.e.* the Hamiltonian H of the system. The Hamiltonian will have kinetic energy (arising from the motion of the spheres) and potential energy (due to sphere-sphere interactions) terms, and we express it as

$$H = \sum_n \left(\frac{1}{2} p_n^2 + W(u_n - u_{n-1}) \right). \tag{4.14}$$

As in previous chapters, u_n denotes the displacement of sphere n from equilibrium. The momentum is given by $p_n = \dot{u}_n \equiv \mathrm{d}u_n/\mathrm{d}t$ and $W(u)$ is the interaction potential between spheres. The following conditions apply to $W(u)$; $W(0) = W'(0) = 0$ and additionally we assume that W'' is positive for small displacements, $W''(0) > 0$. The classical Hamilton equations of motion are written as

$$\dot{u}_n = \frac{\partial H}{\partial p_n}, \quad \dot{p}_n = -\frac{\partial H}{\partial u_n},$$

which lead us to a familiar set of coupled ODEs

$$\ddot{u}_n = -W'(u_n - u_{n-1}) + W'(u_{n+1} - u_n). \tag{4.15}$$

We expand W as a power series

$$W(u) = \sum_m^{\infty} \frac{\phi_m}{m} u^m. \tag{4.16}$$

Considering only small velocities and amplitudes, one can neglect all nonlinear terms from the equations of motion and assume that $\phi_m = 0$ for $m > 2$. Thus, the coupled ODEs are now linear and have the form

$$\ddot{u}_n = \phi_2(u_{n+1} + u_{n-1} - 2u_n). \tag{4.17}$$

The solution to this ODE can be written as a superposition of plane waves where each is given by

$$u_n(t) = A_q \cos(\omega_q t - qn + B_q), \tag{4.18}$$

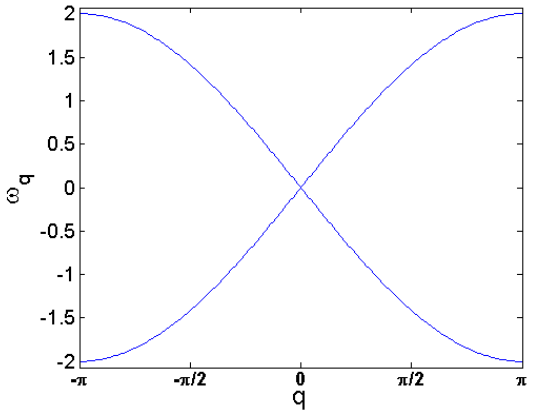

Figure 4.5: A plot of the dispersion relation given by Equation (4.19). The relation is sinusoidal and thus periodic in q with an upper bound given by $|\omega_q| \leq \omega_\pi \equiv 2\sqrt{\phi_2}$ [8]. Figure adapted from Ref.[8].

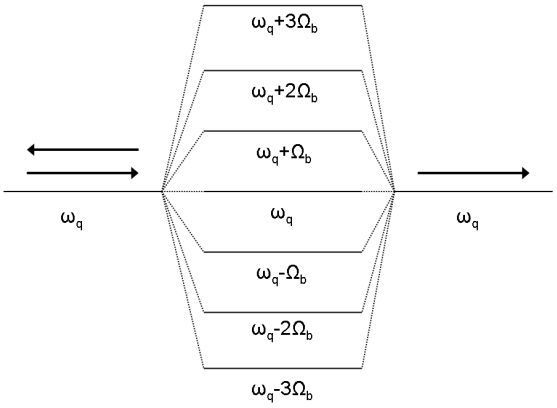

Figure 4.6: A schematic representation of the one-channel scattering of a plane wave by a DB. The breather with frequency Ω_b behaves as a time-periodic potential for the incoming wave of frequency ω_k thus generating new channels.

where ω_q is the plane wave frequency. Here, A_q and B_q are constants. For this system, the dispersion relation is given by Equation (4.19) below and plotted in Figure 4.5

$$\omega_q = \pm 2\sqrt{\phi_2} \sin\left(\frac{q}{2}\right). \tag{4.19}$$

We now consider the DBs themselves. We look for time-periodic DBs, and so seek solutions to Equation (4.15) which have the form

$$\hat{u}_n(t + T_b) = \hat{u}_n(t), \quad \hat{p}_n(t + T_b) = \hat{p}_n(t), \tag{4.20}$$

where $T_b = 2\pi/\Omega_b$ is the period of the DB oscillations. These solutions satisfy the conditions

$$\hat{u}_{n\to\pm\infty} \to c_\pm, \quad \hat{p}_{n\to\pm\infty} \to 0. \tag{4.21}$$

The difference $c_+ - c_-$ characterises the lattice deformation induced by the DB. The first condition above indicates that the DB solution is localised and we choose $c_- = 0$. We can represent $\hat{u}_n$ as a Fourier series expansion with respect to time

$$\hat{u}_n(t) = \sum_{j=-\infty}^{+\infty} A_{jn} \mathrm{e}^{\mathrm{i}k\Omega_b t} \tag{4.22}$$

and the localisation condition given by Equation (4.21) becomes

$$A_{j\neq 0, n\to\pm\infty} \to 0, \quad A_{j=0, n\to\pm\infty} \to c_{\pm}. \tag{4.23}$$

Substituting Equation (4.22) into the original system (4.15), a linearisation of the expressions for A_{jn} and the boundary conditions (4.23) leads to the *nonresonance* condition

$$j\Omega_b \neq \omega_q \tag{4.24}$$

for all i. This condition implies that $\Omega_b > \omega_q$ (excluding the case where $j = 0$).

An important property of localised modes is their stability, which can be analysed by adding a small perturbation to the DB solution $\hat{u}_n$:

$$u_n(t) = \hat{u}_n + \epsilon_n(t)$$

Inserting this expression into Equation (4.15), and retaining only the terms that are linear in ϵ_n, we obtain the first order ODE system

$$\ddot{\epsilon}_n = -W''(\hat{u}_n - \hat{u}_{n-1})(\epsilon_n - \epsilon_{n-1}) + W''(\hat{u}_{n+1} - \hat{n})(\epsilon_{n+1} - \epsilon_n). \tag{4.25}$$

Integration of these equations relate $\epsilon(t)$ and $\dot{\epsilon}(t)$ at $t = T_b$ to the initial conditions at $t = 0$ [4]. It also defines the following map

$$\begin{pmatrix} \epsilon(T_b) \\ \dot{\epsilon}(T_b) \end{pmatrix} = \mathcal{F} \begin{pmatrix} \epsilon(0) \\ \dot{\epsilon}(0) \end{pmatrix} \tag{4.26}$$

where we have defined $\epsilon \equiv (\epsilon_1, \epsilon_2, \dots)$ and $\mathcal{F}$ is a symplectic Floquet matrix. In general,a symplectic matrix A is a square matrix which satisfies $A^T \Gamma A = \Gamma$, where Γ is a nonsingular, skew-symmetric matrix. Floquet theory relates to ODEs which have the form $\dot{x} = B(t)x$, where $B(t)$ is a periodic function. For a detailed discussion of Floquet matrices in the context of DBs see Section VIII.A of Ref.[11]. The eigenvalues λ and eigenvectors $\vec{y}$ of $\mathcal{F}$

provide information on the stability. A DB is said to be linearly stable if all of the eigenvalues of its Floquet matrix $\mathcal{F}$ lie on the unit circle. This means that any small perturbation to the system will not grow exponentially with time [4]. In this case, the eigenvalues can be written as $\mathrm{e}^{\mathrm{i}\theta}$. The eigenvectors are solutions to the Equation (4.25) and satisfy the Bloch condition [16]

$$\epsilon_n(t + T_b) = \mathrm{e}^{-\mathrm{i}\theta}\epsilon_n(t) \tag{4.27}$$

where $\theta = \pm\omega_q T_b$ are the Floquet phases [10]. Using the Bloch condition, we may now write solutions of Equation (4.25) in the form

$$\epsilon_n(t) = \sum_{j=-\infty}^{+\infty} \epsilon_{nj}\mathrm{e}^{\mathrm{i}(\omega_q + j\Omega_b)t}. \tag{4.28}$$

In Section 4.2 we introduced the idea of channels. The DB acts as a time-periodic scattering potential for the incoming wave of frequency ω_q and as such, generates new channels of propagation at frequencies $\omega_q + j\Omega_b$. If $\omega_q + j\Omega_b \neq \omega_{q'}$ for nonzero j then all channels are "closed" except for the "open" channel $j = 0$. This situation corresponds to elastic scattering *i.e.* the energies of the transmitted and reflected waves are equal. Otherwise, the scattering is inelastic [8]. These channels are shown schematically in Figure 4.6.

4.5 Results and Discussion

The simulations performed focused firstly on the interaction of a solitary wave with a DB. The DB used in these simulations has a frequency of 21300 Hz. As in the setups for Chapters 3 and 4, the propagation of a solitary wave is instigated by the impact of a striker. Figure 4.11 consists of various spatio-temporal plots that show the propagation of the solitary wave and its interaction with the DB. The oscillations of the DB can also be clearly seen. Figure 4.9 shows the transmitted amplitude of the solitary wave as a function of striker velocity. Figure 4.10 depicts the ratio of the amplitude of the DB before interaction with the solitary wave to the amplitude after, again as a function of striker velocity. By plotting these figures, we are attempting to gain an understanding of the effect of a DB on the properties of a solitary

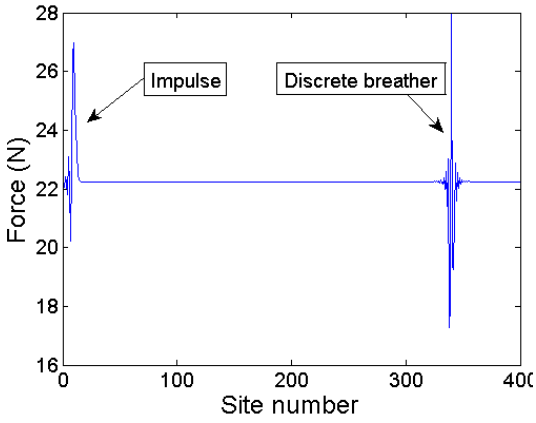

Figure 4.7: The other scenario we study is the interaction of an impulse, generated by a striker, with a DB.

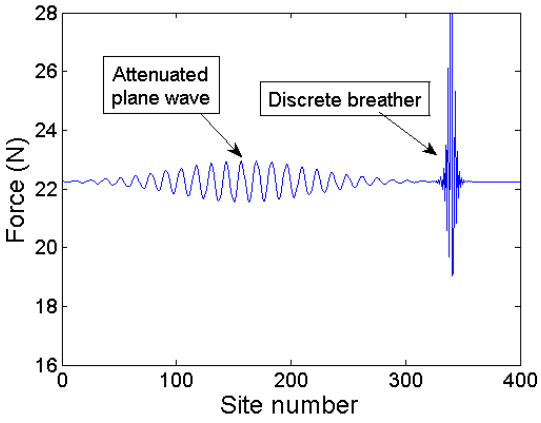

Figure 4.8: This diagram shows the initial setup of our simulation to investigate a plane wave's interaction with a DB.

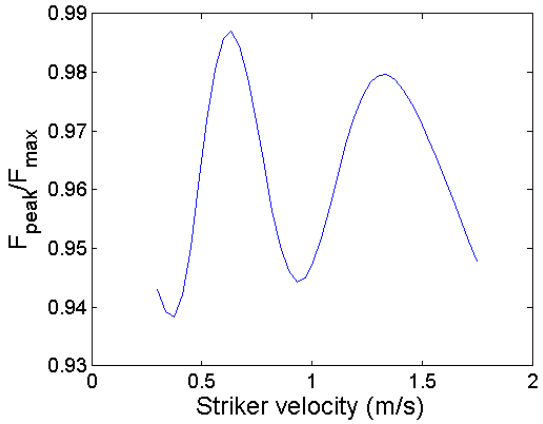

Figure 4.9: The transmitted amplitude of the solitary wave as a function of striker velocity. $F_{\max}$ is the initial amplitude and F_{peak} the amplitude after interaction with the DB.

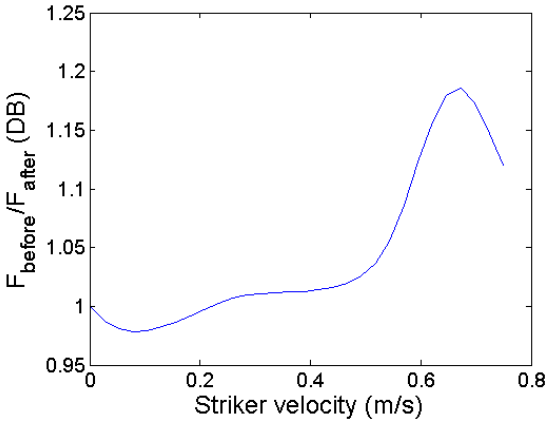

Figure 4.10: The ratio of the maximum amplitude of the DB before interaction with the solitary wave to the maximum amplitude after, as a function of striker velocity.

wave, and *vice versa*. Further research in this area is needed, perhaps using additional DBs and solitary waves of different widths and amplitudes.

Finally, we examine the interaction of an attenuated plane wave with the DB. Our goal is to create a plot analogous to Figure 3 of Ref. [21], which shows the transmission coefficient of a plane wave interacting with a nonlinear impurity mode as a function of wavenumber q. This figure shows the possibility of observing Fano resonances in saturable waveguide arrays. We are interesting in investigating whether a nonlinear analogy of Fano resonance can be observed in our system. Figure 4.8 shows an incoming attenuated plane wave and the DB. The transmitted amplitude as a function of q is given in Figure 4.12. Although there appear to be certain resonances in the system, there is not a direct correspondence between these results and those presented in Figure 3 of Ref. [21]. Consequently, we are unable to confirm whether Fano resonances are possible in this granular system. Further studies will be necessary to investigate this system in greater detail in an effort to explain the features of Figure 4.12.

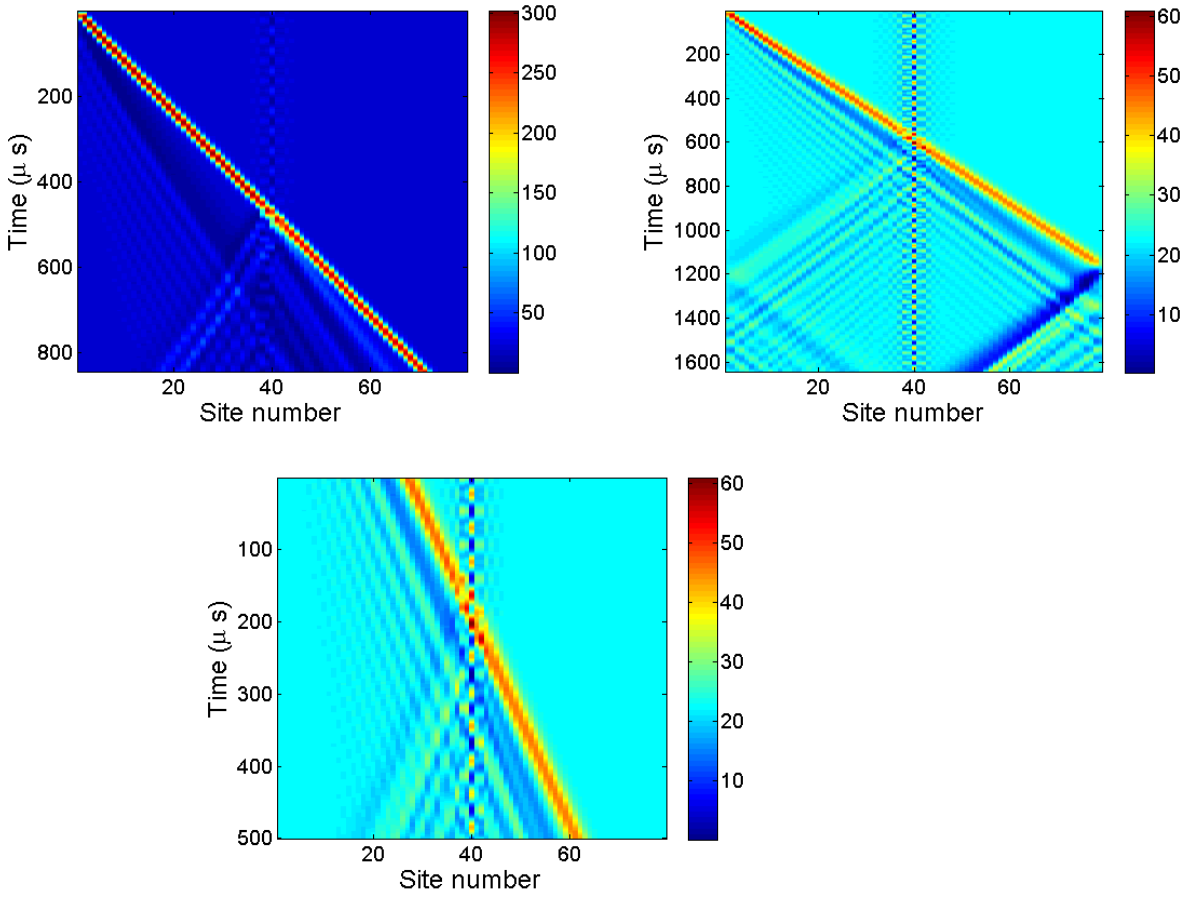

Figure 4.11: These spatio-temporal plots show the propagation of a solitary wave through the lattice and the interaction with a DB. The DB is centered at site forty and we observe the periodic oscillation of this mode. The DB causes partial reflection of the incoming pulse.

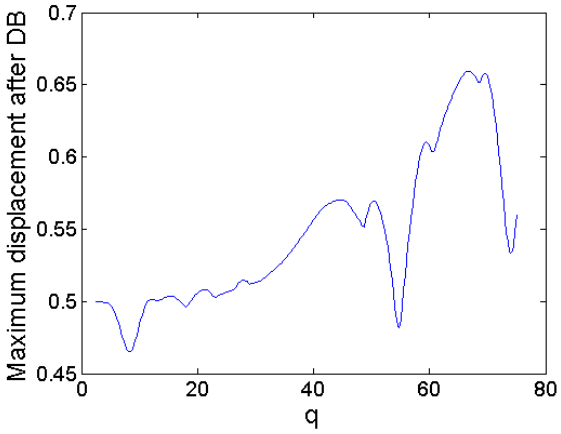

Figure 4.12: We performed simulations using attenuated plane waves with different q values. The transmitted amplitude of this wave was measured and is plotted above.

5 Conclusions

Over the course of this dissertation, we examined the propagation of solitary waves in a variety of granular lattices. In each of the systems that were studied, the sphere interactions were modelled using Hertzian interactions. First, we investigated a chain of uniform steel spheres where a striker was used to instigate the pulse. An approximate solution to the system of coupled ODEs describing the lattice was derived based on the analysis of Chatterjee [2]. The system was also probed using a fourth order Runge-Kutta finite difference scheme that was implemented in MATLAB (see Appendix A). Results of these simulations clearly show the propagation of a non-attenuating, non-dispersive wave through the lattice. We then proceed to derive a relation between wave speed, v_s, and wave amplitude F_{peak} using a scaling analysis. The relation is $v_s \propto F_{\text{peak}}^{1/6}$ and this result is verified by numerics.

The second part of the dissertation studies the role of a defect in the granular lattice. The properties of this defect, *i.e.* the size, Young's modulus E and Poisson ratio ν, are varied and the effect of these variations on the solitary wave's profile are measured. In particular we monitor the amplitude, FWHM and the speed of the wave, and the results are plotted in Figures 3.3 -3.14. Qualitative explanations for several of these curves are provided in Chapter 3. However, some interesting features notably the secondary peak

observed in Figure 3.6 (and to a lesser extent in Figure 3.7) are not clearly understood. A qualitative and quantitative description of these diagrams should be a goal of future work in this area.

In Chapter 4 we introduced the concept of localised modes, specifically DBs. The scattering of plane waves off DBs has been shown to produce interesting resonance phenomena. Work by Naether *et al.* on waveguide arrays had shown that Fano resonance could be observed in these systems [21]. Using this work as a reference, we investigated whether our granular lattice would show similar results. We employed the same numerical setup as that used by Theocharis *et al.* [28] in which a DB is established in the middle of a precompressed chain. We scatter plane waves with varying q off the DB and measure the transmitted amplitude (see Figure 4.12). However, there is not a direct correspondence between these results and those produced by Naether *et al.*. Nevertheless, there appear to be interesting features in Figure 4.12 that we don't yet understand physically and this will be a focus of future work.

A Simulation Code

A MATLAB code is used to simulate our 1D array of spheres. There are four components to the code:

1. The main file
2. A routine containing the fourth-order Runge-Kutta scheme
3. Initialisation file
4. Function to check for contacts between neighbouring spheres

Main file:

```
% This code investigates the case of a chain of steel balls in
% a horizontal row with zero loading (barely touching).

clear all

%%%%%%%%%%%%%%%%%%%%%%%%%%%%%%%%%%%%%%%%%%%%%%%%%%%%%%%%%%%%%%%%%%%%%%%

% DEFINITIONS

time_steps = 40000;
Δ_t = 5e-8;
N = 200; % Number of balls
init_vel = 0.443; % Striker velocity
num_alpha = 1; % Number of alpha values to be tested
defect_pos = 100; % Position of the defect
alpha = linspace(3, 3, num_alpha); %

% We loop over alpha (this is a parameter that varies a
% quantity in our system, e.g. defect radius):

for k = 1:length(alpha)

     % Keep track of how far along the simulation is:
     if ( mod(k,5) == 0 )
         disp(['Step ' int2str(k) ' out of ' ...
             int2str(num_alpha)])
     end

    %%%%%%%%%%%%%%%%%%%%%%%%%%%%%%%%%%%%%%%%%%%%%%%%%%%%%%%%%%%%%%%%%%%%%%%

    % INITIALISATION

```

```
33      %This function creates matrices for position, velocity,
34      %acceleration that will store the values of these
35      %variables for each ball at each step.
36
37      [mass, E, R, poisson, position, velocity, acceleration, ...
38          overlaps, A,...
39          force_30, force_60, distance_30_60] = ...
40          initialise(time_steps, N, init_vel, alpha(k), ...
41          defect_pos);
42
43      %%%%%%%%%%%%%%%%%%%%%%%%%%%%%%%%%%%%%%%%%%%%%%%%%%%%%%%%%%%%%%%%
44      % Iterating forward in time:
45      for i = 2 : time_steps
46
47          %We call a 4th order RK routine which integrates our
48          %equations forward in time:
49          [velocity(i,:), position(i,:), overlaps(i,:)] = ...
50              RK(position(i-1,:), ...
51              velocity(i-1,:), j, N,...
52              R, ...
53              mass, E, poisson, i, Δ_t,...
54              position(1,N), A);
55
56          %Calculate the forces on each ball:
57            force(1,i-1)    = .5*(A(1).*overlaps(i,2).^(3/2));
58            force(N,i-1)    = .5*(A(N-1).*overlaps(i,N).^(3/2));
59            force(2:N-1,i-1)= .5*(A(1:N-2).*overlaps(i,2:N-1)...
60                .^(3/2)+A(2:N-1).*overlaps(3:N).^(3/2));
61
62      end
63
64  end
```

Runge-Kutta routine:

```
1   function [v_new, x_new, overlaps_new] = RK(x_old, v_old, j,...
2       N, R, ...
3       mass, E, poisson, i, Δ_t, Nth_ball_init_pos, A)
4
5   % This function will integrate our equations of motion forward
6   % in time using a 4th order Runge-Kutta method. This is a new
7   % function, based on MAP's code.
8
9   %-------------------------------------------------------------------
10  % Firstly, we must create vectors for the k_x and k_v values:
11  k1_x = zeros(1,N); k1_v = zeros(1,N);
12  k2_x = zeros(1,N); k2_v = zeros(1,N);
13  k3_x = zeros(1,N); k3_v = zeros(1,N);
14  k4_x = zeros(1,N); k4_v = zeros(1,N);
15
```

```
% And we also create a matrix for the overlaps:
k_overlaps = zeros(4, N+1);
%-------------------------------------------------------------------------
% Calculate k1_x:
k1_x = Δ_t * v_old;

% Check for contacts:
[k_overlaps(1, :)] = ...
    contacts(N, Nth_ball_init_pos, x_old, R);

overlaps_new = contacts(N, Nth_ball_init_pos, x_old, R);

% Calculate k1_v:
k1_v(1) = Δ_t*(-(A(1))*k_overlaps(1,2)^(3/2)/mass(1));
k1_v(2:N)=Δ_t*((A(1:(N-1))).*k_overlaps(1,2:N)...
    .^(3/2)./mass(2:N) - ...
    (A(2:N)).*k_overlaps(1,3:(N+1)).^(3/2)./mass(2:N));

%-------------------------------------------------------------------------
% Define the new variables:
xx = x_old + 0.5 * k1_x;
vv = v_old + 0.5 * k1_v;

% Calculate k2_x:
k2_x = Δ_t * vv;

% Check for contacts between balls, using the new xx values:
[k_overlaps(2, :)] = ...
    contacts(N, Nth_ball_init_pos, xx, R);

% Calculate k2_v:
k2_v(1) = Δ_t*(-(A(1))*k_overlaps(2,2)^(3/2)/mass(1));
k2_v(2:N)=Δ_t*((A(1:(N-1))).*k_overlaps(2,2:N)...
    .^(3/2)./mass(2:N) - ...
    (A(2:N)).*k_overlaps(2,3:(N+1)).^(3/2)./mass(2:N));

%-------------------------------------------------------------------------
% Define the new variables:
xx = x_old + 0.5 * k2_x;
vv = v_old + 0.5 * k2_v;

% Calculate k3_x:
k3_x = Δ_t * vv;

% Check for contacts between balls, using the new xx values:
[k_overlaps(3, :)] = ...
    contacts(N, Nth_ball_init_pos, xx, R);

% Calculate k3_v:
k3_v(1) = Δ_t*(-(A(1))*k_overlaps(3,2)^(3/2)/mass(1));
k3_v(2:N)=Δ_t*((A(1:(N-1))).*k_overlaps(3,2:N)...
```

```
67      .^(3/2)./mass(2:N) - ...
68      (A(2:N)).*k_overlaps(3,3:(N+1)).^(3/2)./mass(2:N));
69  %-------------------------------------------------------------------------
70  % Define the new variables:
71  xx = x_old + k3_x;
72  vv = v_old + k3_v;
73
74  % Calculate k4_x:
75  k4_x = Δ_t * vv;
76
77  % Check for contacts between balls, using the new xx values:
78  [k_overlaps(4, :)] = ...
79      contacts(N, Nth_ball_init_pos, xx, R);
80
81  % Calculate k4_v:
82  k4_v(1) = Δ_t*(-(A(1))*k_overlaps(4,2)^(3/2)/mass(1));
83  k4_v(2:N)=Δ_t*((A(1:(N-1))).*k_overlaps(4,2:N)...
84      .^(3/2)./mass(2:N) - ...
85      (A(2:N)).*k_overlaps(4,3:(N+1)).^(3/2)./mass(2:N));
86  %-------------------------------------------------------------------------
87  % Now we go forward in time:
88  v_new = v_old + (1/6) * ( k1_v + 2*k2_v + 2*k3_v +k4_v );
89  x_new = x_old + (1/6) * ( k1_x + 2*k2_x + 2*k3_x +k4_x );
90  %-------------------------------------------------------------------------
```

Initialisation file:

```
1   % This is the initialising function
2
3   function [mass, E, R, poisson, position, velocity, ...
4       acceleration, ...
5       overlaps, A, force_30, force_60, distance_30_60] = ...
6       initialise(time_steps, N, init_vel, alpha, defect_pos)
7
8   %-------------------------------------------------------------------
9   % Parameter definitions
10  rho_steel = 7780; % Density of steel
11  rho_PTFE = 2178; % Density of PTFE
12  rho_brass = 8500; % Density of brass
13  E_steel = 1.93*10^11; % Young's mod for steel
14  E_rubber = 30000000; % Young's mod for rubber
15  E_brass = 1.03 * 10^11;
16  E_PTFE = 1.46*10^9;
17  rad = 0.00476/2; % Ball radius
18  poisson_steel = 0.3; % Poisson ratio for steel
19  poisson_rubber = 0.49; % Poisson ratio for rubber
20  poisson_brass = 0.34;
21  poisson_PTFE = 0.46;
22  %-------------------------------------------------------------------
23  %Creating vectors which will store the material properties
```

```
%of the balls
mass = zeros(1,N);
E = zeros(1,N); %Young's modulus
R = zeros(1,N); %Radius
poisson = zeros(1,N); %Poisson ratio
%-------------------------------------------------------------------
% All steel balls
for i = 2 : N
    E(i) = E_steel;
    R(i) = rad;
    poisson(i) = poisson_steel;% Value for steel
    mass(i) = 0.00045;% Value for steel
end

% Insert 1 defect (steel ball):
R(defect_pos) = alpha * rad;
mass(defect_pos) = (4/3) * pi * (R(defect_pos)^3)...
    * rho_steel;
E(defect_pos) = E_steel;
poisson(defect_pos) = poisson_steel;

%The first ball (the striker) is made from steel
E(1) = E_steel;
R(1) = rad;
poisson(1) = poisson_steel;
mass(1) = 0.00045;

%We give the wall ball an 'infinite' radius, and it's
%made from brass
E(N+1) = E_brass;
%R(N+1) = 1000;
poisson(N+1) = poisson_brass;
%mass(N) = (4/3)*pi*rho_steel*(R(N))^3;

%%%%%%%%%%%%%%%%%%%%%%%%%%%%%%%%%%%%%%%%%%%%%%%%%%%%%%%%%%%%%%%%

%Creating the matrices that will store the variables
position = zeros(N,time_steps)';
velocity = zeros(N,time_steps)';
acceleration = zeros(N,time_steps)';

%We also create a matrix to store the overlaps between
%neighbouring balls. This will have N columns, and a row for
%each time step. Initially, due to our placement of the balls,
%all overlaps will be zero.
overlaps = zeros(N+1,time_steps)';
%The overlap of the 1st ball with its left neighbour is always
%zero:
overlaps(:,1) = 0;

% Putting the balls in position (all equilibrium positions are
```

```
% initially zero, no loading in the system)
position(1,1) = 0;

% Initialising the velocities:
% The first ball in the chain is given an initial velocity,
% the others are all at rest (so just need
% to change this first value)

velocity(1,1) = init_vel;

% All accelerations initially zero, so we don't have to do
% anything

% We may also calculate all the force coefficients at this
% point:
A = zeros(1, N);

A(1:(N-1)) = 4*E(1:(N-1)).*E(2:N).*sqrt(R(1:(N-1)))...
    .*R(2:N)./
    (R(1:(N-1))+R(2:N))).^(3*E(2:N).*...
        (1-poisson(1:(N-1)).^2)+
    3*E(1:(N-1)).*(1-poisson(2:N).^2));
A(N) = (4*E(N)*E(N+1)*sqrt(R(N)))/(3*E(N+1)*...
    (1-poisson(N)^2) +
    3*E(N)*(1-poisson(N+1)^2));

end
```

Contact checking function:

```
% We determine whether any balls are overlapping
function [new_overlaps] = contacts(N, Nth_ball_init_pos, xx, R)

new_overlaps = zeros(1,N+1);

% The first ball has no overlap on its LHS
    new_overlaps(1) = 0;

% We now calculate the overlaps of the other balls
    new_overlaps(2:N) = max( 0, xx(1:(N-1)) - xx(2:N) );

% Dealing with the Nth-ball/wall interaction
    new_overlaps(N+1) = max(0, xx(N) - 0);
```

References

[1] R. Carretero-González, D. Khatri, M.A. Porter, P.G. Kevrekidis, and C. Daraio. Dissipative Solitary Waves in Granular Crystals. *Physical Review Letters*, 102(2):024102, 2009.

[2] A. Chatterjee. Asymptotic Solution for Solitary Waves in a Chain of Elastic Spheres. *Physical Review E*, 59(5):5912–5919, 1999.

[3] C. Coste, E. Falcon, and S. Fauve. Solitary waves in a chain of beads under hertz contact. *Physical Review E*, 56(5):6104–6117, 1997.

[4] T. Cretegny, S. Aubry, and S. Flach. 1d Phonon Scattering by Discrete Breathers. *Physica D*, 119(1-2):73 – 87, 1998.

[5] C. Daraio, V. F. Nesterenko, E. B. Herbold, and S. Jin. Strongly nonlinear waves in a chain of teflon beads. *Physical Review E*, 72(1):016603, 2005.

[6] U. Fano. Effects of configuration interaction on intensities and phase shifts. *Phys. Rev.*, 124(6):1866–1878, 1961.

[7] E. Fermi, J. Pasta, and S. Ulam. Studies of Nonlinear Problems. I. *Los Alamos Scientific Laboratory*, Report LA-1940, 1955.

[8] S. Flach and A. Gorbach. Discrete Breathers in Fermi–Pasta–Ulam lattices. *Chaos*, 15(1):015112, 2005.

[9] S. Flach and A. V. Gorbach. Discrete Breathers – Advances in theory and applications. *Physics Reports*, 467(1-3):1 – 116, 2008.

[10] S. Flach, A. E. Miroshnichenko, and M. V. Fistul. Wave scattering by Discrete Breathers. *Chaos*, 13(2):596–609, 2003.

[11] S. Flach and C. R. Willis. Discrete Breathers. *arXiv:patt-sol/9704004v1*, 1997.

[12] E. Hascoët and H.J. Herrmann. Shocks in Non-Loaded Bead Chains with Impurities. *The European Physical Journal B*, 14(1):183 – 190, 2000.

[13] J. Hong and A. Xu. Nondestructive identification of impurities in granular medium. *Applied Physics Letters*, 81(25):4868–4870, 2002.

[14] S. Job, F. Melo, A. Sokolow, and S. Sen. Solitary wave trains in granular chains: Experiments, Theory and Simulations. *Granular Matter*, 10(1):13–20, 2007.

[15] S. Job, F. Santibanez, F. Tapia, and F. Melo. Wave Localization in strongly nonlinear Hertzian chains with mass defect. *arXiv:0901.3532v1*, 2009.

[16] Charles Kittel. *Introduction to Solid State Physics*. Wiley, New York, 1996.

[17] L.D. Landau and E.M. Lifschitz. *Theory of Elasticity*. Pergamon, Oxford, 1970.

[18] A.E.H. Love. *A Treatise on the Mathematical Theory of Elasticity*. Dover, New York, Fourth edition, 2003.

[19] I. G. Main. *Vibrations and Waves in Physics*. CUP, Cambridge, Third edition, 1993.

[20] A. E. Miroshnichenko, S. Flach, and Y. S. Kivshar. Fano resonances in nanoscale structures. *arXiv:0902.3014v4*, 2009.

[21] U. Naether, D. E. Rivas, M. A. Larenas, M. I. Molina, and R. A. Vicencio. Fano resonances in saturable waveguide arrays. *arXiv:0906.1160v2*, 2009.

[22] V. F. Nesterenko. *Dynamics of Heterogeneous Materials*. Springer-Verlag, New York, 2001.

[23] V.F. Nesterenko. Propagation of Nonlinear Compression Pulses in Granular Media. *Journal of Applied Mechanics and Technical Physics*, 24(5):733 – 743, 1983.

[24] L. Ponson, N. Bocchler, Y. Ming Lai, M.A. Porter, P.G. Kevrekidis, and C. Daraio. Elastic Spin Chains. *arXiv:0904.0426v1*, 2009.

[25] M. A. Porter, C. Daraio, I. Szelengowicz, E. B. Herbold, and P.G. Kevrekidis. Highly nonlinear solitary waves in heterogeneous periodic granular media. *Physica D*, 238(6):666 – 676, 2009.

[26] M.A. Porter, N.J. Zabusky, B. Hu, and D.K. Campbell. Fermi, Pasta, Ulam and the Birth of Experimental Mathematics. *American Scientist*, 97(6):214–221, 2009.

[27] S. Sen, J. Hong, J. Bang, E. Avalos, and R. Doney. Solitary Waves in the Granular Chain. *Physics Reports*, 462(2):21 – 66, 2008.

[28] G. Theocharis, M. Kavousanakis, P.G. Kevrekidis, C. Daraio, M.A. Porter, and I.G. Kevrekidis. Localized Breathing Modes in Granular Crystals with Defects. *arXiv:0906.4094v1*, 2009.

[29] P. Tong, B. Li, and B. Hu. Wave transmission, phonon localization, and heat conduction of a one-dimensional Frenkel-Kontorova chain. *Physical Review B*, 59(13):8639–8645, 1999.

[30] G. B. Whitham. *Linear and Nonlinear Waves*. John Wiley & Sons, 1974.